Int. J. Fuzzy Syst.
https://doi.org/10.1007/s40815-023-01466-5

Stabilization of Photovoltaic Systems with Fuzzy Event-Triggered Communication

R. Vadivel[1] · T. K. Santhosh[3] · B. Unyong[2] · Quanxin Zhu[4] · Jinde Cao[5] · Nallappan Gunasekaran[6]

Received: 7 July 2022 / Revised: 5 November 2022 / Accepted: 9 January 2023

Abstract This article addresses the study of a photovoltaic system for type-2 interval fuzzy models via event-triggered control (ETC). Compared to similar works initiated in the references, the necessary part of modeling the ETC for the photovoltaic system ($\mathscr{PV}$) is to produce the maximum path which should be followed to guarantee the most extreme power activity. The system models are expected to depend on uncertain parameters, which are mostly experienced in the real dynamical system. To describe the $\mathscr{PV}$ system with event-triggered communication delay, the behavior of a nonlinear system can be addressed by using the interval type-2 (IT2) Takagi–Sugeno (T–S) fuzzy rules with lower and upper membership functions. In this regard, we construct the suitable Lyapunov– Krasovskii functional (LKF) and integral inequalities to achieve the stability conditions and expand the maximum sampling period of the closed-loop system. The main purpose of this study is to design the event-triggered mechanism such that the resulting closed-loop system is asymptotically stable and to reduce the communication burdens of the $\mathscr{PV}$ system. For this, a sufficient condition is derived for the proposed system in the form of linear matrix inequalities (LMIs). Finally, simulation results are given to demonstrate the suitability and merits of the newly suggested techniques.

Keywords Event-triggered control · Lyapunov–Krasovskii functional · Linear matrix inequality · Photovoltaic system

1 Introduction

The world's energy requests and needs are continuously increasing, and tremendous examination has been conducted and exploited to create and use sustainable power, which has the necessity of being adaptable, reliable, and non-polluting. The imperative force is to utilize an

✉ Quanxin Zhu
zqx22@126.com

R. Vadivel
vadivelsr@yahoo.com

T. K. Santhosh
tksanthosh.kct@gmail.com

B. Unyong
bundit.un@wu.ac.th

Jinde Cao
jdcao@seu.edu.cn

Nallappan Gunasekaran
gunasmaths@gmail.com

[1] Department of Mathematics, Faculty of Science and Technology, Phuket Rajabhat University, Phuket 83000, Thailand

[2] Department of Mathematics, School of Science, Walailak University, Nakhon Si Thammarat 80160, Thailand

[3] School of Electrical and Electronics Engineering, SASTRA Deemed University, Thanjavur, India

[4] School of Mathematics and Statistics, Hunan Normal University, Changsha, China

[5] School of Mathematics, Southeast University, Nanjing 210096, China

[6] Computational Intelligence Laboratory, Toyota Technological Institute, Nagoya 468-8511, Japan

Published online: 08 March 2023

economical and effective source of energy to minimize fuel supply issues to ensure our current environment [1–3]. There are 789 million people around the globe without access to electricity, according to the United Nations report published in 2018. To provide energy access to all, the United Nations has set an ambitious goal of providing affordable, reliable, and sustainable energy access to all by 2030 as part of the 17 sustainable development goals [4]. The transition to renewable energy is already occurring with the addition of a global capacity of 200 GW occurring in 2019 [5]. The share of renewable energy sources in energy generation has increased significantly in recent years, as several governments consider this a genuine effort to reduce emissions. Among the renewable energy sources (sun-based, wind, and geothermal, and so on), the solar-based photovoltaic ($\mathscr{PV}$) energy was generally used in numerous usages [6–9] because of its benefits-direct electric power form, ease of service, etc. Likewise, an enormous financial benefit and the incredible development of traction execution can be gained if $\mathscr{PV}$ is carried out throughout the control. When extracting electrical force, numerous productive attempts are generally known, along with maximum power point (MPP) tracking methods, for instance, perturb, observe technique [10, 11], etc. Authors in [12] investigated the problem of photovoltaic grid-connected power systems via type-2 fuzzy model in terms of adaptive event-triggered saturation control. Identification of the optimal operating point of $\mathscr{PV}$ system via NN for real-time MPP tracking control has been studied in [13]. In particular, an interesting stability analysis of power systems with the penetration of $\mathscr{PV}$-based generation has been examined in [14]. Consequently, the achievement of the $\mathscr{PV}$ system from various appearances has been studied in [12–14], in particular, an event-triggered control (ETC) the scheme was attracted recently. However, there are only a few examinations considering the stability analysis of the $\mathscr{PV}$ system, see [1] and [12, 14].

In addition, Takagi–Sugeno (T–S) fuzzy model has brought a lot of research attention in the course of recent years since they have been perceived as the most well-known and fruitful way to deal with nonlinear dynamical systems. The main property of the T–S fuzzy model is that the general dynamics of the smooth nonlinear system can be portrayed as simple linear subsystems using membership functions. Due to this reality, many impressive results on nonlinear systems have been developed using the T–S fuzzy model approach [15–18]. Different from them, the interval type-2 Takagi–Sugeno (IT2 T–S) fuzzy system can be used to express uncertain nonlinear systems through the convex simulation of linear systems. Traditional type-1 fuzzy systems are based on type-1 fuzzy set theory, which can settle nonlinearities very well. However, it is not particularly suitable to solve the system uncertainties which widely exist in the practical systems [19]. Compared with type-1 fuzzy systems, the membership functions of IT2 fuzzy systems are dynamic and can be adjusted online [20, 21]. Thus, the IT2 fuzzy systems are much more suitable to solve the problem of the uncertain systems than the type-1 fuzzy systems. Therefore, it has found extensive applications in several fields in recent years [20–22]. Recently, the researchers from the control community have lost sight of the type-2 fuzzy area and a fruitful result have been developed. The authors of [23] investigated the observer-based fuzzy ETC for IT2 fuzzy systems. The problem of the IT2 fuzzy system with the sampled data controller (SDC) has been discussed in [24]. Recently, Ref. [17] examined the finite-time extended dissipativity control for IT2 fuzzy systems with resilient memory SDC. Furthermore, most of the literature works based on $\mathscr{PV}$ system have been concentrated on type-1 T–S fuzzy schemes, and the study of ETC has not been included in those results. As a result, the $\mathscr{PV}$ system with ETC is significant from a theoretical perspective and has extraordinary practical applications. Along these lines, it is of useful significance to analyze the execution activity and stability analysis of systems with uncertain parameters [25]. To address the problem, various investigations have been conducted with respect to the stability issues of time-varying delays in the models of the nonlinear system [26] and [27]. In [21, 23, 24], the IT2 fuzzy methodologies have been proposed, where the uncertainty information and ETC mechanism of the considered system have not been presented in the references. To develop the stability examination of the communication delay, various strategies have been considered in the published works, for instance, the free weight matrix technique, limited Bessel–Legendre inequality approaches, etc.

Since the ETC transmits feedback signals only when the current signal satisfies the present criterion, this has the advantages of less energy consumption, and fewer tasks being executed. Compared with the traditional time-triggered mechanism, the event-triggered mechanism performs tasks only when the system's state exceeds the given threshold condition. Therefore, the ETC has attracted more attention and achieved great progress in recent years. Moreover, ETC, primarily composed of an event generator and a feedback controller, has been widely considered because it can guarantee system behavior and minimize the number of transmitted packets [22, 28, 29]. ETC has many benefits to minimizing data transmission, and network pressure, and saving limited network bandwidth [30–32]. Authors in [33], studied H_∞ fuzzy state-feedback control synthesis for $\mathscr{PV}$ systems. In [34], we investigated the MPP tracking controller for $\mathscr{PV}$ systems using fuzzy models. Recently, observer-based event-triggered stabilization (ET) for IT2 fuzzy systems has been examined in

[31]. In view of MPP tracking techniques, the authors of [35] employed the sliding mode control strategy to address the problem for grid-connected $\mathscr{PV}$ systems. In contrast to existing controller methods in the literature based on the $\mathscr{PV}$ system, how our proposed ETC reduces the communication load without performance degradation compared to conventional controllers. In this manner, we propose the combination of a DC/DC Boost converter and ETC mechanism to regulate the power output by controlling state and state-derivative variables of the $\mathscr{PV}$ system. However, a photovoltaic system for type-2 interval fuzzy models with ETC has not been well addressed yet, which is the main motivation of this paper.

With reference to the above discussion, we endeavor to investigate the ETC for $\mathscr{PV}$ systems with the IT2 fuzzy model in this paper. By employing the matrix inequality approaches, adequate conditions are verified to ensure the robust asymptotic stability conditions and the desired controller gains are given in reference to linear matrix inequalities (LMIs). The main contributions are listed as follows:

(i) An ETC is proposed in the IT2 fuzzy model with simple rules and is used to describe the dynamical behaviors of the $\mathscr{PV}$ system.
(ii) To ensure the robust asymptotically stable conditions of the proposed $\mathscr{PV}$ system under the new LKF with some novel integral inequalities and the LMI method.
(iii) The desired robust ETC gain matrices for the considered system can be determined with the suggested LMI condition using the MATLAB toolbox.
(iv) The adequacy of the suggested approaches is demonstrated by numerical examples with some simulation in the end.

Notations for a matrix S, S^{-1} indicates the inverse and S^{T} represents the transpose, $\mathbb{R}^m$ and $\mathbb{R}^{n\times m}$ denote the m-dimensional Euclidean space and the set of the real matrix $n \times m$, respectively. For $\mathscr{Y}$ is a positive (negative) definite matrix, such that $\mathscr{Y} > 0, (\mathscr{Y} < 0)$, I_n stands for identity matrix of dimension n, mathematical expectation $\mathbb{E}\{\cdot\}$ denotes the stochastic process, $*$ in a symmetric matrix indicates the entry means symmetry, $\mathrm{Sym}\{X\} = X + X^{\mathrm{T}}$, and $\mathbb{N}$ represents the set of positive integers.

2 Problem Formation and Preliminaries

2.1 Modeling of Photo-voltaic ($\mathscr{PV}$) Current

Considered the $\mathscr{PV}$ output current is given as follows:

$$\iota_{\mathscr{PV}} = v_\alpha \hat{I}_{\alpha k} - v_\alpha \hat{I}_n \left(\exp\left[\frac{w(V_{\mathscr{PV}} + M_n \iota_{\mathscr{PV}})}{K\mathscr{T}E} \right] - 1 \right) - \frac{\mathscr{V}_{\mathscr{PV}} + l_{\mathscr{PV}} M_n}{M_{nk}}, \tag{1}$$

where $\hat{I}_{\alpha k}$ and $\hat{I}_n$ denote the light-generated current and the cell saturation of the dark current, respectively. $V_{\mathscr{PV}}$ and $\iota_{\mathscr{PV}}$ are the $\mathscr{PV}$ output voltage and current of $\mathscr{PV}$, respectively. M_n and M_{nk} are the cell series and shunt resistances, respectively. $w, K, \mathscr{T}, v_\alpha$ and E are denoted as electron charge, Boltzmann constant, cell temperature, number of parallel solar cells, and ideal factor, respectively. Figure 1 illustrates the structure of the basic solar energy conversation system. The light-generated current relies upon solar irradiation and cell temperature with the accompanying expression as

$$\hat{I}_{\alpha k} = Q(\hat{I}_{nf} + K_1(\mathscr{T} - \mathscr{T}_s)), \tag{2}$$

where $\hat{I}_{nf}$ denotes the cell short-circuit current. $K_1, \mathscr{T}_s$ and Q noted as cell short-circuit current temperature coefficient, cell reference temperature, and solar irradiation in kW/m^2, respectively. In addition, the saturation current depends on the cell temperature defined as follows:

$$\hat{I}_n = \hat{I}_{\mathrm{rn}} \left(\frac{T}{T_s} \right)^3 \exp\left[\frac{w\Xi_v}{KE} \left(\frac{1}{T_s} - \frac{1}{\mathscr{T}} \right) \right], \tag{3}$$

where Ξ_v is the band-gap energy of the semiconductor used in the cell and $\hat{I}_{\mathrm{rn}}$ is the reverse saturation current and can be defined by:

$$\hat{I}_{\mathrm{rn}} = \frac{\hat{I}_{nf}}{\exp\left[\frac{wV_{\mathrm{of}}}{v_n KTM} \right] - 1}. \tag{4}$$

Here, V_{of} represents the open-circuit voltage.

2.2 Boost Converter Model

The DC/DC boost converter dynamic behavior can be characterized as follows:

$$\begin{cases} \dot{\iota}_{\mathscr{L}} &= -\dfrac{M_{\mathscr{L}}}{\mathscr{L}} \iota_{\mathscr{L}} + \dfrac{1}{\mathscr{L}} \mathscr{V}_{\mathscr{PV}} - \dfrac{\mathscr{Y}}{\mathscr{L}} (\mathscr{V}_0 + v_{\mathrm{d}} - M_{\mathrm{a}} \iota_{\mathscr{V}}), \\ \dot{\mathscr{V}}_{\mathscr{PV}} &= -\dfrac{1}{\hat{C}_1} \iota_{\mathscr{L}} + \dfrac{1}{\hat{C}_1} \iota_{\mathscr{PV}}, \end{cases} \tag{5}$$

where $\iota_{\mathscr{L}}$, $\mathscr{I}_0$, $\mathscr{V}_0$, and $\mathscr{Y}$ are the boost self-inductance current, output load current, output load voltage, and control input corresponding to the duty cycle. $\hat{C}_1, \hat{C}_2, \mathscr{L}, M_{\mathrm{a}}, M_{\mathscr{L}}, v_{\mathrm{d}}$ are the input capacitor, output capacitor, boost inductance, self-inductance resistance, and resistance characterized by loss in the MOSFET state and forward voltage drop of the

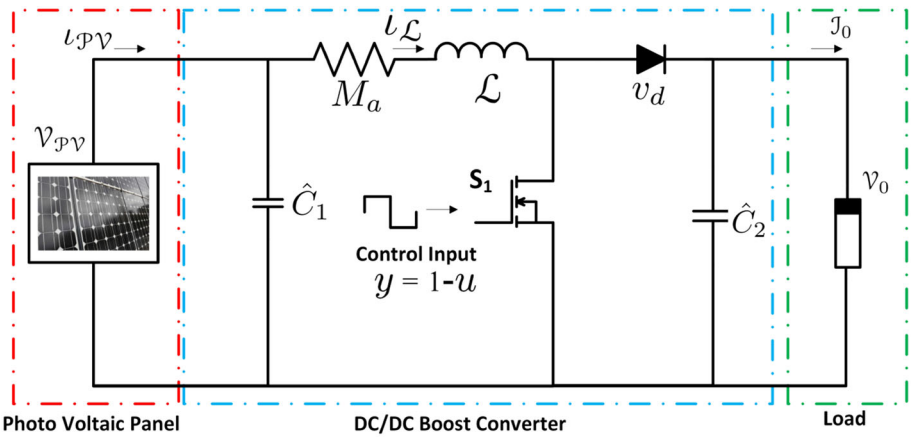

Fig. 1 Solar energy conversion system

diode, respectively. Utilizing (5) and including the new state variable, for example $\dot{u} = u_{\mathscr{P}\mathscr{V}}$, the system $\mathscr{P}\mathscr{V}$ can be explained by the following nonlinear model:

$$\dot{\varrho}(t) = g(\varrho(t)) + \mathscr{B}u(t), \tag{6}$$

where

$$g(\varrho(t)) = \begin{bmatrix} -\frac{M_{\mathscr{L}}}{\mathscr{L}}\iota_{\mathscr{L}} + \frac{1}{\mathscr{L}}\mathscr{V}_{\mathscr{P}\mathscr{V}} - \frac{\mathscr{y}}{\mathscr{L}}(\mathscr{V}_0 + v_{\mathrm{d}} - M_{\mathrm{a}}\iota_{\mathscr{L}})u_{\mathscr{P}\mathscr{V}} \\ -\frac{1}{\hat{C}_1}\iota_{\mathscr{L}} \\ 0 \end{bmatrix},$$

$$\varrho = \begin{bmatrix} \iota_{\mathscr{L}} \\ \mathscr{V}_{\mathscr{P}\mathscr{V}} \\ u_{\mathscr{P}\mathscr{V}} \end{bmatrix}, \quad \mathscr{B} = \begin{bmatrix} 0 \\ \frac{1}{\hat{C}_1}\iota_{\mathscr{P}\mathscr{V}} \\ 0 \end{bmatrix}.$$

2.3 Interval Type-2 Fuzzy System of the Photo-voltaic Model

In order to formulate the event-triggered controller, the $\mathscr{P}\mathscr{V}$ nonlinear (6) can be written as by using the output load voltage $\mathscr{V}_0$ and the boost inductance current $\iota_{\mathscr{L}}$:

$$\dot{\varrho}(t) = \mathscr{A}(\iota_{\mathscr{L}}, \mathscr{V}_0)\varrho(t) + \mathscr{B}u(t), \tag{7}$$

where

$$\mathscr{A}(\iota_{\mathscr{L}}, \mathscr{V}_0) = \begin{bmatrix} -\frac{M}{\mathscr{L}} & \frac{1}{\mathscr{L}} & -\frac{\mathscr{V}_0 + v_{\mathrm{d}} - M_{\mathrm{a}}\iota_{\mathscr{L}}}{\mathscr{L}} \\ -\frac{1}{\hat{C}_1} & 0 & 0 \\ 0 & 0 & 0 \end{bmatrix}, \quad \mathscr{B} = \begin{bmatrix} 0 \\ \frac{1}{\hat{C}_1} \\ 0 \end{bmatrix}.$$

Defining $\iota_{\mathscr{L}}, \mathscr{V}_0$ bounded as $\alpha \le \iota_{\mathscr{L}} \le \beta$ and $\gamma \le \mathscr{V}_0 \le \delta$. Now, the nonlinear system can be stated with respect to linear subsystems according to T–S fuzzy IF–THEN rules is as follows.

Rule i: **IF** $h_1(\varrho(t))$ is G_1^i and $\cdots$ and $h_r(\varrho(t))$ is G_r^i **THEN**

$$\dot{\varrho}(t) = \mathscr{A}_i\varrho(t) + \mathscr{B}_i u(t), \quad (i = 1, 2, \ldots, \mathcal{Q}) \tag{8}$$

with $h(\varrho(t)) = [h_1(\varrho(t)), \ldots, h_r(\varrho(t))]$ denotes the variable in the premises and $G_j^i (i = 1, \ldots, \mathcal{Q}; j = 1, \ldots, r)$ represents the IT2 fuzzy set for ith rule and $\mathcal{Q}$ indicate the number of fuzzy rules. The firing the interval of the ith rule is represented as

$$\begin{aligned} \mathbb{X}_i(\varrho(t)) &= \left[\prod_{j=1}^{\mathcal{Q}} \underline{\tau}_{G_j^i}(h_j(\varrho(t))), \prod_{j=1}^{\mathcal{Q}} \overline{\tau}_{G_j^i}(h_j(\varrho(t)))\right], \\ &= [\underline{\mathscr{X}}_i(\varrho(t)), \overline{\mathscr{X}}_i(\varrho(t))], \quad i = 1, 2, \ldots, \mathcal{Q}, \end{aligned} \tag{9}$$

where $0 \le \underline{\tau}_{G_j^i}(h_j(\varrho(t))) \le 1$ and $0 \le \overline{\tau}_{G_j^i}(h_j(\varrho(t))) \le 1$ denote the lower and upper membership functions. $\underline{\mathscr{X}}_i(\varrho(t))$ and $\overline{\mathscr{X}}_i(\varrho(t))(0 \le \underline{\mathscr{X}}_i(\varrho(t))) \le \overline{\mathscr{X}}_i(\varrho(t))$ are the lower and upper grades of the membership function. The inferred IT2 T–S fuzzy model is described by

$$\dot{\varrho}(t) = \sum_{i=1}^{\mathcal{Q}} \tilde{\mathscr{X}}_i(\varrho(t))(\mathscr{A}_i\varrho(t) + \mathscr{B}_i u(t)), \tag{10}$$

where $\tilde{\mathscr{X}}_i(\varrho(t)) = \underline{\lambda}_i(\varrho(t))\underline{\mathscr{X}}_i(\varrho(t)) + \overline{\lambda}_i(\varrho(t))\overline{\mathscr{X}}_i(\varrho(t))$, in which $\sum_{i=1}^{\mathcal{Q}} \tilde{\mathscr{X}}_i(\varrho(t)) = 1$. The weight coefficient function satisfies $\underline{\lambda}_i(\varrho(t)) + \overline{\lambda}_i(\varrho(t)) = 1, \underline{\lambda}_i(\varrho(t)) \in [0, 1], \overline{\lambda}_i(\varrho(t)) \in [0, 1]$.

2.4 Event-Triggered Scheme

Throughout this work, we choose the system (10) that is controlled through the network. Now, inspired by [32], the following event-triggered mechanism is introduced. Suppose the current release time is l_s, the sampled state is denoted as $\varrho(l_{\mathrm{sd}})$ and the current sampled state can be noted as $\varrho(l_{\mathrm{sd}} + \jmath d)$ with $d > 0$ being a constant fulfills the subsequent event-triggered conditions

$$\begin{aligned}&(\varrho(l_{\mathrm{sd}}+\jmath d),\varrho(l_{\mathrm{sd}}))=[\varrho(l_{\mathrm{sd}}+\jmath d)-\varrho(l_{\mathrm{sd}})]^{\mathrm{T}}\tilde{\Theta}_1\\&\quad[\varrho(l_{\mathrm{sd}}+\jmath d)-\varrho(l_{\mathrm{sd}})]-\chi\varrho^{\mathrm{T}}(l_{\mathrm{sd}})\tilde{\Theta}_2\varrho(l_{\mathrm{sd}})>0,\quad \jmath\in\mathbb{N}.\end{aligned}\tag{11}$$

Moreover, the data transmitted between l_s and l_{s+1} satisfy

$$(\varrho(l_{\mathrm{sd}}+\jmath d),\varrho(l_{\mathrm{sd}}))\le 0,\tag{12}$$

where $\tilde{\Theta}_1>0$ and $\tilde{\Theta}_2>0$ are symmetric matrices, and

$$l_{s+1}=l_s+\min_{\jmath}\{\jmath|(\varrho(l_{\mathrm{sd}}+\jmath d),(l_{\mathrm{sd}}))\}.\tag{13}$$

Here, we choose two more consecutive event instants $t=l_{\mathrm{sd}}$ and $t=l_{s+1}d$ to demonstrate the execution mechanism of the event triggered. At $t=l_sd$, the sensor send the information to state $\varrho(l_sd)$ to the controller. Meanwhile, the sensor determines the event condition (11) in periodic time instant $t=l_sd+\jmath d(\jmath\in\mathbb{N})$ with respect to the information on the real-time state information $\varrho(l_sd+\jmath d)$ and the last transmitted $\varrho(l_sd)$. When the condition (11) is identified, the sensor allows new data $\varrho(l_sd+\jmath d)$ to be sent to the controller and causes a new instant of events $t=l_{s+1}d=l_sd+\jmath d$. Therefore, the release instants sequence of sensor can be expressed as $\{t=l_sd|s\in\mathbb{N}\}$. It is supposed that without data dropout, the sampled-data transmission happens, but transmission delays cannot be ignored. Moreover, the delay $\eta_1\le\eta(t_s)\le\eta_2$ indicates the sth sample state released transmission between the event-triggered scheme and the zero-order hold (ZOH). Taking into the account of network-induced delay, the following IT2 T–S fuzzy controller is designed for the system (10), where its jth rule is given as follows. *Rule j:* **IF** $h_1(\varrho(t))$ is G_1^j and $\cdots$ and $h_r(\varrho(t))$ is G_r^j

THEN

$$u(t)=\mathbb{K}_j\varrho(l_sd),t\in[l_sd+\eta_{l_s},l_{s+1}d+\eta_{l_{s+1}}),\tag{14}$$

where $\mathbb{K}_j$ are the control gain matrices and will be calculated later. The network-induced delay is indicated as $\eta_{l_s}\in[\eta_1,\eta_2),s\in\mathbb{N}$. From the general discussion, the system (10) converts in terms of the time-delay model. First, we divide the time interval as $[l_s+\eta_{l_s},l_{s+1}+\eta_{l_{s+1}})$ into $l_{s+1}-l_s$ consecutive subintervals.

$$\begin{aligned}&[l_sd+\eta_{l_s},l_{s+1}d+\eta_{l_{s+1}})\\&\quad=\bigcup_{v=0}^{l_s}[l_sd+vd+\eta_{l_s+v},l_sd+(v+1)d+\eta_{l_s+v+1}),\end{aligned}$$

where η_{l_s+v} denoted as scalar. When $v=0,\eta_{l_s+v}=\eta_{l_s}$ and $v=1,\eta_{l_s+v}=\eta_{l_s+1}$. With the information on the membership function, the following fuzzy IT2 T–S ETC is defined as

$$u(t)=\sum_{j=1}^{\mathcal{Q}}(\underline{\mathscr{X}}_j^1(\varrho(l_sd))+\overline{\mathscr{X}}_j^1(\varrho(l_sd)))\mathbb{K}_j\varrho(l_sd),$$

with

$$\underline{\mathscr{X}}_j^1(\varrho(l_sd))=\frac{\underline{\mathscr{X}}_j(\varrho(l_sd))}{\sum_{j=1}^{\mathcal{Q}}(\underline{\mathscr{X}}_j(\varrho(l_sd))+\overline{\mathscr{X}}_j(\varrho(l_sd)))}\ge 0,$$

$$\overline{\mathscr{X}}_j^1(\varrho(l_sd))=\frac{\overline{\mathscr{X}}_j(\varrho(l_sd))}{\sum_{j=1}^{\mathcal{Q}}(\underline{\mathscr{X}}_j(\varrho(l_sd))+\overline{\mathscr{X}}_j(\varrho(l_sd)))}\ge 0$$

and fulfill the following property $\sum_{j=1}^{\mathcal{Q}}(\underline{\mathscr{X}}_j^1(\varrho(l_sd))+\overline{\mathscr{X}}_j^1(\varrho(l_sd)))=1$. In view of average normalized membership grades of the lower and upper membership functions, the suggested IT2 fuzzy controller is designed, say, the normalized central (NC) fuzzy controller scheme. Define piecewise $\eta(t):=t-l_{\mathrm{sd}}$ and $e(t):=\varrho(l_sd)-\varrho(l_sd+vd)$, we get $\eta_1\le\eta(t)\le\eta_2$. Then, the entire IT2 T–S fuzzy ETC is

$$u(t)=\sum_{j=1}^{\mathcal{Q}}\tilde{\mathscr{X}}_j^1\varrho(l_sd)\mathbb{K}_j(\varrho(t-\eta(t))-e(t)),\tag{15}$$

where $\tilde{\mathscr{X}}_j^1(\varrho(l_sd)=(\underline{\mathscr{X}}_j^1(\varrho(l_sd))+\overline{\mathscr{X}}_j^1(\varrho(l_sd)))$. Finally, ETC $\mathscr{PV}$ system can be stated in the subsequent form:

$$\begin{aligned}\dot{\varrho}(t)=&\sum_{i=1}^{\mathcal{Q}}\tilde{\mathscr{X}}_i(\varrho(t))\sum_{j=1}^{\mathcal{Q}}\tilde{\mathscr{X}}_j^1(\varrho(l_sd)(\mathscr{A}_i\varrho(t)\\&+\mathscr{B}_i\mathbb{K}_j(\varrho(t-\eta(t))-e(t))),\end{aligned}\tag{16}$$

Remark 2.1 As a result of the earlier discussion, the $\mathscr{PV}$ system (10) is transformed into a time-delay modeled system in view of networked induced delay. From (11) and the analysis of $\eta(t)$ and $e(t)$, we defined as follows:

$$\begin{aligned}e^{\mathrm{T}}(t)\tilde{\Theta}_1e(t)\le\kappa_1[\varrho(t-\eta(t))-e(t)]^{\mathrm{T}}\\\tilde{\Theta}_2[\varrho(t-\eta(t))-e(t)],\quad\kappa_1\in[0,1)].\end{aligned}\tag{17}$$

As indicated by the state conditions characterized in (16), the $\mathscr{PV}$ system with IT2 fuzzy models with parameter uncertainties can be defined as

$$\begin{aligned}\dot{\varrho}(t)=&\sum_{i=1}^{\mathcal{Q}}\tilde{\mathscr{X}}_i(\varrho(t))\sum_{j=1}^{\mathcal{Q}}\tilde{\mathscr{X}}_j^1(\varrho(l_sd)(\hat{\mathscr{A}}_i\varrho(t)\\&+\hat{\mathscr{B}}_i\mathbb{K}_j(\varrho(t-\eta(t))-e(t))),\end{aligned}\tag{18}$$

where $\hat{\mathscr{A}}_i=\mathscr{A}_i+\Delta\mathscr{A}_i$ and $\hat{\mathscr{B}}_i=\mathscr{B}_i+\Delta\mathscr{B}_i$. $\Delta\mathscr{A}_i$ and $\Delta\mathscr{B}_i$ are noted as adjustable matrices

$$\Delta\mathscr{A}_i=\mathbb{E}_i\mathbb{F}(t)\mathbb{V}_{1i},\quad\Delta\mathscr{B}_i=\mathbb{E}_i\mathbb{F}(t)\mathbb{V}_{2i},$$

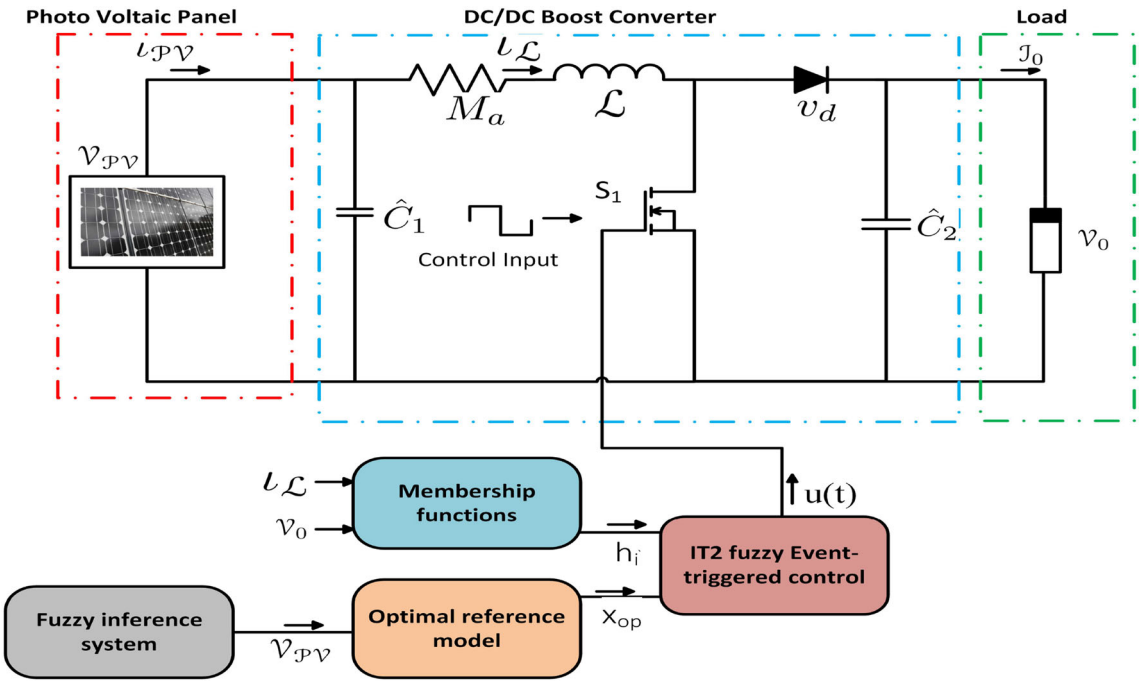

Fig. 2 $\mathscr{PV}$ based ETC for the IT2 T–S fuzzy systems

where $\mathbb{E}_i, \mathbb{V}_{1i}$, and $\mathbb{V}_{2i}$ are known matrices with adjustable dimensions, $\mathbb{F}(t)$ is unknown real time-varying matrices satisfies $\mathbb{F}^{\mathrm{T}}(t)\mathbb{F}(t) \leq I$, where all the elements $\mathbb{F}(t)$ are Lebesgue measurable. The objective of this study is to develop a robust asymptotically stable criterion for the proposed ETC $\mathscr{PV}$ system (18). As a result, the block diagram of the proposed IT2 fuzzy design-based ETC $\mathscr{PV}$ system is shown in Fig. 2. To this end, we initiate the subsequent definition and lemmas.

Lemma 2.2 [27] *For a differentiable function* $r : [\alpha, \beta] \to \mathbb{R}^n$, *a positive integer* $k \in \mathbb{N}$, $m \in \mathbb{Z}_{\geq 0}$, *a matrix* $R \in \mathbb{R}^{n\times n} > 0$, *a vector* $\xi \in \mathbb{R}^{kn}$, *and adjustable matrices* $N_s \in \mathbb{R}^{kn\times n}$ $(s = 1, \ldots, m+1)$. *Then inequality becomes a given.*

$$-\int_{\alpha}^{\beta} \dot{r}^{\mathrm{T}}(s)R\dot{r}(s)\mathrm{d}s \leq \sum_{i=1}^{m+1} \frac{\beta-\alpha}{2i-1}\xi^{\mathrm{T}}N_iR^{-1}N_i + \mathrm{Sym}(N_i\psi_{i-1}(\alpha,\beta))\xi, \tag{19}$$

where

$$\psi_i(\alpha,\beta) = \begin{cases} r(\beta) - r(\alpha), i = 0; \\ r(\beta) - (-1)^i r(\alpha) - \sum_{j=1}^{i} l_j^i \frac{j!}{(\beta-\alpha)^j}\rho_{(j-1)} \cdot \rho_m(\alpha,\beta) \\ (\alpha,\beta), i \in \mathbb{N}, \end{cases}$$
$$= \int_{s_o}^{\beta}\int_{s_1}^{\beta}\cdots\int_{s_m}^{\beta} r(s_{m+1})ds_{m+1}\cdots ds_1, \quad s_o = \alpha;$$
$$l_j^i = (-1)^{j+i}\binom{i}{j}\binom{i+j}{j}.$$

Lemma 2.3 [26] *For any matrices* $\mathscr{X}, \mathscr{Y}$ *and symmetric matrices* $\mathscr{G}_1 > 0, \mathscr{S} > 0$, *and* $\mathscr{W} > 0$, *then the following condition holds for the function* $\rho(t)$ *in* $[\alpha, \beta]$:

$$\int_{\alpha}^{\beta} \dot{\rho}^{\mathrm{T}}(s)\mathscr{G}_1\dot{\rho}(s)\mathrm{d}s \geq \sigma^{\mathrm{T}}\begin{bmatrix} (\alpha-\beta)\mathscr{S} & \mathscr{X}[I\ 0] \\ * & \frac{(\alpha-\beta)}{3}\mathscr{W} + \mathrm{Sym}(\mathscr{Y}[I\ -2I]) \end{bmatrix}\sigma, \tag{20}$$

where σ_1 is any vector and $\sigma_2 = [\rho^{\mathrm{T}}(\beta) - \rho^{\mathrm{T}}(\alpha), \rho^{\mathrm{T}}(\beta) - \frac{1}{(\alpha-\beta)}\int_{\alpha}^{\beta}\rho^{\mathrm{T}}(s)\mathrm{d}s]^{\mathrm{T}}, \sigma = [\sigma_1^{\mathrm{T}}\ \sigma_2^{\mathrm{T}}]^{\mathrm{T}}$.

Lemma 2.4 [25] *Let* $Y, \mathscr{H}$ *and* $J(t)$ *be the matrices of adjustable dimensions, and* $J(t)$ *satisfying* $J^{\mathrm{T}}(t)J(t) \leq I$, *the subsequent inequality being true for any constant* $\epsilon > 0$:

$$YJ(t)\mathscr{H} + \mathscr{H}^{\mathrm{T}}J^{\mathrm{T}}(t)Y^{\mathrm{T}} \leq \epsilon YY^{\mathrm{T}} + \epsilon^{-1}\mathscr{H}^{\mathrm{T}}\mathscr{H}.$$

Lemma 2.5 [25] *For matrices* $\mathscr{R} > 0$, $X^{\mathrm{T}} = X$ *and any scalar* ρ. *Then the following condition is true*:

$$-XR^{-1}X = \rho^2\mathscr{R} - 2\rho X.$$

Remark 2.6 Let the differentiable function $\bar{r} : \left[\hat{\alpha}, \hat{\beta}\right] \to \mathbb{R}^n$, a positive integer $k \in \mathbb{N}$, a matrix $R \in \mathbb{R}^{n\times n}$, any vector $\xi \in \mathbb{R}^{kn}$, and adjustable matrices $N_s \in \mathbb{R}^{kn\times n}$ $(s = p, q)$, the following conditions are true:

$$-\int_{\hat{\alpha}}^{\hat{\beta}} \dot{\bar{r}}^{\mathrm{T}}(s)R\dot{\bar{r}}(s)\mathrm{d}s \le \xi^{\mathrm{T}}\Big[(\hat{\beta}-\hat{\alpha})\Big(N_pR^{-1}N_p^{\mathrm{T}} + \frac{1}{3}N_qR^{-1}N_q^{\mathrm{T}}\Big) + \mathrm{Sym}(N_p\mathbb{E}_1 + N_q\mathbb{E}_2)\Big]\xi, \tag{21}$$

where

$$\mathbb{E}_1\xi = r(\hat{\beta}) - r(\hat{\alpha}), \mathbb{E}_2\xi = \bar{r}(\hat{\beta}) + \bar{r}(\hat{\alpha}) - \frac{2}{\hat{\beta}-\hat{\alpha}}\int_{\hat{\alpha}}^{\hat{\beta}} \bar{r}(s)\mathrm{d}s.$$

3 Main Results

In this part, we aim to determine the ETC law such that the $\mathscr{PV}$ system (18) guarantees the robust asymptotically stable. In this manner, a suitable LKF, and by using inequality techniques a criterion that stabilizes the considered IT2 T–S fuzzy $\mathscr{PV}$ system (18).

Theorem 3.1 *For given control gain matrices $\mathbb{K}_j$, and positive scalars $\eta_1, \eta_2, \lambda_1, \lambda_2, \kappa_1$, the described $\mathscr{PV}$ system (18) is robust asymptotically stable, if there exist common matrices* $\mathbb{P} \in \mathbb{R}^{4n\times 4n} > 0$, $\mathbb{Q}_1 > 0$, $\mathbb{Q}_2 > 0$, $\mathbb{G}_1 > 0$, $\mathbb{G}_2 > 0$, $\mathbb{S}_1 > 0$, $\mathbb{G}_3 > 0$, $\mathscr{S} \in \mathbb{R}^{3n\times 3n}$, $\mathscr{X} \in \mathbb{R}^{3n\times n}$, $\mathscr{Y} \in \mathbb{R}^{2n\times n}$, $\mathscr{W} \in \mathbb{R}^{2n\times 2n}$, $\mathbb{Y}$, $\mathbb{T}$, *and any matrix* $\mathbb{N}_h \in \mathbb{R}^{5n\times n}, \mathbb{M}_h \in \mathbb{R}^{5n\times n}$, $\tilde{\Theta}_1$, $\tilde{\Theta}_2$, $h = 1, 2$, *and* $\eta(t) \in \{\eta_1, \eta_2\}$ *satisfying the following LMIs*:

$$\bar{\Phi}_1 = \begin{bmatrix} \Psi & \bar{\mathbb{W}} & \Psi_{13} & \Psi_{14} & \mathbb{S}_1\hat{\Gamma}_1^{\mathrm{T}} & \tilde{\Lambda}_{11} \\ * & -\frac{1}{\eta_2}\mathbb{G}_3 & 0 & 0 & 0 & 0 \\ * & * & -\eta_1\mathbb{G}_1 & 0 & 0 & 0 \\ * & * & * & -\eta_{12}\mathbb{G}_2 & 0 & 0 \\ * & * & * & * & -\mathbb{S}_1 & 0 \\ * & * & * & * & * & \tilde{\Lambda}_{22} \end{bmatrix} < 0, \tag{22a}$$

$$\bar{\Phi}_2 = \begin{bmatrix} \Psi & \bar{\mathbb{W}} & \Psi_{13} & \Psi_{14} & \mathbb{S}_1\hat{\Gamma}_1^{\mathrm{T}} & \tilde{\tilde{\Lambda}}_{11} \\ * & -\frac{1}{\eta_2}\mathbb{G}_3 & 0 & 0 & 0 & 0 \\ * & * & -\eta_1\mathbb{G}_1 & 0 & 0 & 0 \\ * & * & * & -\eta_{12}\mathbb{G}_2 & 0 & 0 \\ * & * & * & * & -\mathbb{S}_1 & 0 \\ * & * & * & * & * & \tilde{\Lambda}_{22} \end{bmatrix} < 0, \tag{22b}$$

where

$\tilde{\Lambda}_{11} = [\eth_1\ \eth_2\ \eth_3\ \eth_4\ \eth_5\ \eth_6\ \eth_7]$, $\tilde{\tilde{\Lambda}}_{11} = [\eth_1\ \hat{\eth}_2 hat\eth_3\ \eth_4\ \eth_5\ \eth_6\ \eth_7]$,
$\eth_2 = [(\eta_2 - \eta(t))\mathbb{M}_1\ \underbrace{0\ 0\ 0}_{7\ times}]$, $\eth_3 = [(\eta_2 - \eta(t))\mathbb{M}_2\ \underbrace{0\ 0\ 0}_{7\ times}]$,
$\hat{\eth}_2 = [(\eta(t) - \eta_1)\mathbb{N}_1\ \underbrace{0\ 0\ 0}_{7\ times}], \eth_1 = [\eta_2\mathbb{G}_3\hat{\Gamma}_1^{\mathrm{T}}\ \underbrace{0\ 0\ 0}_{7\ times}]$
$\hat{\eth}_3 = [(\eta(t) - \eta_1)\mathbb{N}_2\ \underbrace{0\ 0\ 0}_{7\ times}], \eth_4 = \Gamma_{\mathrm{d}}$, $\eth_5 = \lambda_1\Gamma_e^{\mathrm{T}}$,
$\eth_6 = V_e$, $\eth_7 = \lambda_2 V_e^{\mathrm{T}}, \Psi_{13} = \eta_1\mathbb{G}_1\hat{\Gamma}_1^{\mathrm{T}}$, $\Psi_{14} = \eta_{12}\mathbb{G}_2\hat{\Gamma}_1^{\mathrm{T}}$
$\tilde{\Lambda}_{22} = \mathrm{diag}\{-\eta_2\mathbb{G}_3\ -\mathbb{G}_2\ -3\mathbb{G}_2\ -\lambda_1 I\ -\lambda_1 I\ -\lambda_2 I - \lambda_2 I\}$, $\Psi = \Big[\mathrm{Sym}(\varphi_1^{\mathrm{T}}\mathbb{P}\varphi_2) + \varsigma_1^{\mathrm{T}}\mathbb{Q}_1\varsigma_1 - \varsigma_2^{\mathrm{T}}\mathbb{Q}_1\varsigma_2 + \varsigma_2^{\mathrm{T}}\mathbb{Q}_2\varsigma_2 - \varsigma_4^{\mathrm{T}}\mathbb{Q}_2\varsigma_4 - \eta_{12}\Big(\mathrm{Sym}(\mathbb{N}_1\mathbb{E}_1 + \mathbb{N}_2\mathbb{E}_2) + \mathrm{Sym}(\mathbb{M}_1\mathbb{E}_3 + \mathbb{M}_2\mathbb{E}_4)\Big) + \Upsilon_{1,1}^{\mathrm{T}}\bigtriangledown_1\Upsilon_{1,1} - \frac{\pi^2}{4}[(\varsigma_1 - \varsigma_2)^{\mathrm{T}}\ \mathbb{S}_1(\varsigma_1 - \varsigma_2) + 2[\varsigma_1^{\mathrm{T}}\mathbb{Y} + \varsigma_4^{\mathrm{T}}\mathbb{T}][\varsigma_1 - \varsigma_4] + \kappa_1[\varsigma_3 - \varsigma_1]^{\mathrm{T}}\tilde{\Theta}_2[\varsigma_3 - \varsigma_1] - \varsigma_1^{\mathrm{T}}\tilde{\Theta}_1\varsigma_1, \varphi_2 = [\varsigma_s^{\mathrm{T}}\ \varsigma_1^{\mathrm{T}} - \varsigma_2^{\mathrm{T}}\ \varsigma_2^{\mathrm{T}}\ -\varsigma_4^{\mathrm{T}}]^{\mathrm{T}}$,
$\varphi_1 = [\varsigma_1^{\mathrm{T}}\ \eta_1\varsigma_5^{\mathrm{T}}\ (\eta(t) - \eta_1)\varsigma_6^{\mathrm{T}}\ (\eta_2 - \eta(t))\varsigma_7^{\mathrm{T}}]^{\mathrm{T}}$,
$\varsigma_s = \mathscr{A}_i\varsigma_1 + \mathscr{B}_i\mathbb{K}_j\varsigma_3 - \mathscr{B}_i\mathbb{K}_j\varsigma_4$, $\bar{\mathbb{W}} = [\mathbb{Y}^{\mathrm{T}}\ 0\ 0\ \mathbb{T}^{\mathrm{T}}\ \underbrace{0\ 0\ 0}_{4\ times}]^{\mathrm{T}}$,
$\hat{\Gamma}_1^{\mathrm{T}} = [\mathscr{A}_i\ 0\ \mathscr{B}_i\mathbb{K}_j\underbrace{0\ 0\ 0}_{4\ times}\ -\mathscr{B}_i\mathbb{K}_j]^{\mathrm{T}}$, $\eta_{12} = \eta_2 - \eta_1$,
$\eta_1(t) = \eta(t) - \eta_1$, $\eta_2(t) = \eta_2 - \eta(t)$, $\mathbb{E}_1 = \varsigma_2 - \varsigma_3$,
$\mathbb{E}_2 = \varsigma_2 + \varsigma_3 - 2\varsigma_6$, $\mathbb{E}_3 = \varsigma_3 - \varsigma_4$, $\mathbb{E}_4 = \varsigma_3 + \varsigma_4 - 2\varsigma_7$,
$\varsigma_l = [0_{n\times(l-1)n}\ I_n\ 0_{n\times(8-l)n}]$, $l = 1, 2, \ldots, 8$.

Proof We choose the following LKF candidate as follows:

$$V(t) = \sum_{l=1}^{3} V_l(t), \tag{23}$$

where

$$V_1(t) = \bar{\theta}^{\mathrm{T}}(t)\mathbb{P}\bar{\theta}(t) + \int_{t-\eta_1}^{t} \varrho^{\mathrm{T}}(s)\mathbb{Q}_1\varrho(s)\mathrm{d}s + \int_{t-\eta_2}^{t-\eta_1} \varrho^{\mathrm{T}}(s)\mathbb{Q}_2\varrho(s)\mathrm{d}s,$$
$$V_2(t) = \int_{t-\eta_1}^{t}\int_{\theta}^{t} \dot{\varrho}^{\mathrm{T}}(s)\mathbb{G}_1\dot{\varrho}(s)\mathrm{d}s\mathrm{d}\theta + \int_{t-\eta_2}^{t}\int_{\theta}^{t} \dot{\varrho}^{\mathrm{T}}(s) \times \mathbb{G}_3\dot{\varrho}(s)\mathrm{d}s\mathrm{d}\theta + (\eta_2 - \eta_1)\int_{t-\eta_2}^{t-\eta_1}\int_{\theta}^{t} \dot{\varrho}^{\mathrm{T}}(s)\mathbb{G}_2\dot{\varrho}(s)\mathrm{d}s\mathrm{d}\theta,$$
$$V_3(t) = \int_{t-\eta(t)}^{t} \dot{\varrho}^{\mathrm{T}}(s)\mathbb{S}_1\dot{\varrho}(s)\mathrm{d}s - \frac{\pi^2}{4}\int_{t-\eta(t)}^{t} (\varrho(s) - \varrho(s-\eta(s)))^{\mathrm{T}}\mathbb{S}_1(\varrho(s) - \varrho(s-\eta(s)))\mathrm{d}s,$$
$$\bar{\theta}(t) = \Big[\varrho^{\mathrm{T}}(t)\ \int_{t-\eta_1}^{t} \varrho^{\mathrm{T}}(s)\mathrm{d}s\ \int_{t-\eta(t)}^{t-\eta_1} \varrho^{\mathrm{T}}(s)\mathrm{d}s\ \int_{t-\eta_2}^{t-\eta(t)} \varrho^{\mathrm{T}}(s)\mathrm{d}s\Big]^{\mathrm{T}}.$$

Taking derivation on $V(t)$, we get

$$\dot{V}(t) = \dot{V}_1(t) + \dot{V}_2(t) + \dot{V}_3(t),$$

where

$$\begin{aligned}\dot{V}_1(t) &= 2\bar{\theta}^{\mathrm{T}}(t)\mathbb{P}\dot{\bar{\theta}}(t) + \varrho^{\mathrm{T}}(t)\mathbb{Q}_1\varrho(t) - \varrho^{\mathrm{T}}(t-\eta_1)\mathbb{Q}_1\varrho(t-\eta_1)\\ &\quad + \varrho^{\mathrm{T}}(t-\eta_1)\mathbb{Q}_2\varrho(t-\eta_1) - \varrho^{\mathrm{T}}(t-\eta_2)\mathbb{Q}_2\varrho(t-\eta_2)\\ &= \chi^{\mathrm{T}}(t)\big\{\mathrm{Sym}(\varphi_1^{\mathrm{T}}\mathbb{P}\varphi_2) + \varsigma_1^{\mathrm{T}}\mathbb{Q}_1\varsigma_1 - \varsigma_2^{\mathrm{T}}\mathbb{Q}_1\varsigma_2\\ &\quad + \varsigma_2^{\mathrm{T}}\mathbb{Q}_2\varsigma_2 - \varsigma_4^{\mathrm{T}}\mathbb{Q}_2\varsigma_4\big\}\chi(t),\end{aligned} \tag{24}$$

where

$$\begin{aligned}\chi^{\mathrm{T}}(t) &= \Bigg[\varrho^{\mathrm{T}}(t)\ \varrho^{\mathrm{T}}(t-\eta_1)\ \varrho^{\mathrm{T}}(t-\eta(t))\ \varrho^{\mathrm{T}}(t-\eta_2)\\ &\quad \frac{1}{\eta_1}\int_{t-\eta_1}^{t}\varrho^{\mathrm{T}}(s)\mathrm{d}s\ \frac{1}{\eta_1(t)}\int_{t-\eta(t)}^{t-\eta_1}\varrho^{\mathrm{T}}(s)\mathrm{d}s\\ &\quad \frac{1}{\eta_2(t)}\int_{t-\eta_2}^{t-\eta(t)}\varrho^{\mathrm{T}}(s)\mathrm{d}s\ e^{\mathrm{T}}(t)\Bigg],\\ \dot{V}_2(t) &= \dot{\varrho}^{\mathrm{T}}(t)(\eta_1\mathbb{G}_1 + \eta_{12}^2\mathbb{G}_2 + \eta_2\mathbb{G}_3)\dot{\varrho}(t)\\ &\quad - \int_{t-\eta_1}^{t}\dot{\varrho}^{\mathrm{T}}(s)\mathbb{G}_1\dot{\varrho}(s)\mathrm{d}s - \int_{t-\eta_2}^{t}\dot{\varrho}^{\mathrm{T}}(s)\mathbb{G}_3\dot{\varrho}(s)\mathrm{d}s\\ &\quad - \eta_{12}\int_{t-\eta_2}^{t-\eta_1}\dot{\varrho}^{\mathrm{T}}(s)\mathbb{G}_2\dot{\varrho}(s)\mathrm{d}s.\end{aligned}$$

Utilizing (21) and evaluate $-\eta_{12}\int_{t-\eta_2}^{t-\eta_1}\dot{\varrho}^{\mathrm{T}}(s)\mathbb{G}_2\dot{\varrho}(s)\mathrm{d}s$, we get

$$\begin{aligned}&-\eta_{12}\int_{t-\eta_2}^{t-\eta_1}\dot{\varrho}^{\mathrm{T}}(s)\mathbb{G}_2\dot{\varrho}(s)\mathrm{d}s = -\int_{t-\eta(t)}^{t-\eta_1}\dot{\varrho}^{\mathrm{T}}(s)\mathbb{G}_2\dot{\varrho}(s)\mathrm{d}s\\ &\quad - \int_{t-\eta_2}^{t-\eta(t)}\dot{\varrho}^{\mathrm{T}}(s)\mathbb{G}_2\dot{\varrho}(s)\mathrm{d}s\\ &\quad \le \eta_{12}\chi^{\mathrm{T}}(t)\Bigg[(\eta(t)-\eta_1)\Bigg(\mathbb{N}_1\mathbb{G}_2^{-1}\mathbb{N}_1^{\mathrm{T}} + \frac{1}{3}\mathbb{N}_2\mathbb{G}_2^{-1}\mathbb{N}_2^{\mathrm{T}}\Bigg)\\ &\quad + \mathrm{Sym}(\mathbb{N}_1\mathbb{E}_1 + \mathbb{N}_2\mathbb{E}_2) + (\eta_2-\eta(t))\big(\mathbb{M}_1\mathbb{G}_2^{-1}\mathbb{M}_1^{\mathrm{T}}\\ &\quad + \frac{1}{3}\mathbb{M}_2\mathbb{G}_2^{-1}\mathbb{M}_2^{\mathrm{T}}\Bigg) + \mathrm{sym}(\mathbb{M}_1\mathbb{E}_3 + \mathbb{M}_2\mathbb{E}_4)\Bigg]\chi(t).\end{aligned}$$

Using the Lemma 2.3 for the first integral term in $\dot{V}_2(t)$, we have

$$-\int_{t-\eta_1}^{t}\dot{\varrho}^{\mathrm{T}}(s)\mathbb{G}_1\dot{\varrho}(s)\mathrm{d}s \le \Upsilon_{1,1}^{\mathrm{T}}\bigtriangledown_1\Upsilon_{1,1},$$

where

$$\Upsilon_{1,1}^{\mathrm{T}} = \begin{bmatrix}\hat{\alpha}_1\\ \hat{\alpha}_2\end{bmatrix}^{\mathrm{T}},\quad \bigtriangledown_1 = \begin{bmatrix}\eta_1\mathscr{S} & \mathscr{X}[I\ 0]\\ * & \frac{\eta_1}{3}\mathscr{W} + \mathrm{sym}(\mathscr{Y}[I\ -2I])\end{bmatrix},$$
$$\hat{\alpha}_1^{\mathrm{T}} = [\varsigma_1^{\mathrm{T}}\ \varsigma_2^{\mathrm{T}}\ \varsigma_5^{\mathrm{T}}],\quad \hat{\alpha}_2 = [\varsigma_1^{\mathrm{T}} - \varsigma_2^{\mathrm{T}}\ \varsigma_1^{\mathrm{T}} - \varsigma_5^{\mathrm{T}}]. \tag{25}$$

Therefore, we can obtain

$$\begin{aligned}\dot{V}_2(t) &\le \chi^{\mathrm{T}}(t)\Bigg[\Upsilon_{1,1}^{\mathrm{T}}\bigtriangledown_1\Upsilon_{1,1} - \eta_{12}\Bigg((\eta(t)-\eta_1)\big(\mathbb{N}_1\mathbb{G}_2^{-1}\mathbb{N}_1^{\mathrm{T}}\\ &\quad + \frac{1}{3}\mathbb{N}_2\mathbb{G}_2^{-1}\mathbb{N}_2^{\mathrm{T}}\Bigg) + \mathrm{Sym}(\mathbb{N}_1\mathbb{E}_1 + \mathbb{N}_2\mathbb{E}_2)\\ &\quad + (\eta_2-\eta(t))\Bigg(\mathbb{M}_1\mathbb{G}_2^{-1}\mathbb{M}_1^{\mathrm{T}} + \frac{1}{3}\mathbb{M}_2\mathbb{G}_2^{-1}\mathbb{M}_2^{\mathrm{T}}\Bigg)\\ &\quad + \mathrm{Sym}(\mathbb{M}_1\mathbb{E}_3 + \mathbb{M}_2\mathbb{E}_4)\Bigg)\Bigg],\\ \dot{V}_3(t) &\le \dot{\varrho}^{\mathrm{T}}(t)\mathbb{S}_1\dot{\varrho}(t) - \frac{\pi^2}{4}[(\varrho(t)-\varrho(t-\eta(t)))^{\mathrm{T}}\\ &\quad \times \mathbb{S}_1(\varrho(t)-\varrho(t-\eta(t))]\chi(t).\end{aligned} \tag{26}$$

Combining all the derivatives with (17) and letting $\mathbb{W}^{\mathrm{T}} = [\mathbb{Y}^{\mathrm{T}},\ \mathbb{T}^{\mathrm{T}}]$ we get

$$\begin{aligned}\dot{V}(t) &\le \sum_{i=1}^{\mathcal{Q}}\tilde{\mathscr{X}}_i(\varrho(t))\sum_{j=1}^{\mathcal{Q}}\tilde{\mathscr{X}}_i^1(\varrho(l_sd)\chi^{\mathrm{T}}(t)\Big[\mathrm{Sym}(\varphi_1^{\mathrm{T}}\mathbb{P}\varphi_2)\\ &\quad + \varsigma_1^{\mathrm{T}}\mathbb{Q}_1\varsigma_1 - \varsigma_2^{\mathrm{T}}\mathbb{Q}_1\varsigma_2 + \varsigma_2^{\mathrm{T}}\mathbb{Q}_2\varsigma_2\\ &\quad - \varsigma_4^{\mathrm{T}}\mathbb{Q}_2\varsigma_4 - \eta_{12}\Big((\eta(t)-\eta_1)\big(\mathbb{N}_1\mathbb{G}_2^{-1}\mathbb{N}_1^{\mathrm{T}}\\ &\quad + \frac{1}{3}\mathbb{N}_2\mathbb{G}_2^{-1}\mathbb{N}_2^{\mathrm{T}}\Big) + \mathrm{Sym}(\mathbb{N}_1\mathbb{E}_1 + \mathbb{N}_2\mathbb{E}_2) + (\eta_2-\eta(t))\\ &\quad \times\Bigg(\mathbb{M}_1\mathbb{G}_2^{-1}\mathbb{M}_1^{\mathrm{T}} + \frac{1}{3}\mathbb{M}_2\mathbb{G}_2^{-1}\mathbb{M}_2^{\mathrm{T}}\Bigg) + \mathrm{Sym}(\mathbb{M}_1\mathbb{E}_3\\ &\quad + \mathbb{M}_2\mathbb{E}_4)\Big) + \Upsilon_{1,1}^{\mathrm{T}}\bigtriangledown_1\Upsilon_{1,1} + \dot{\varrho}^{\mathrm{T}}(t)\mathbb{S}_1\dot{\varrho}(t)\\ &\quad - \frac{\pi^2}{4}[(\varrho(t)-\varrho^{\mathrm{T}}(t-\eta(t))\mathbb{S}_1(\varrho(t)-\varrho(t-\eta(t)]\\ &\quad + 2[\varrho^{\mathrm{T}}(t)\mathbb{Y} + \varrho^{\mathrm{T}}(t-\eta_2)\mathbb{T}]\times[\varrho(t)-\varrho(t-\eta_2)\\ &\quad - \int_{t-\eta_2}^{t}\dot{\varrho}(s)\mathrm{d}s] + \kappa_1[\varrho(t-\eta(t)) - e(t)]^{\mathrm{T}}\tilde{\Theta}_2\\ &\quad \times[\varrho(t-\eta(t)) - e(t)] - e^{\mathrm{T}}(t)\tilde{\Theta}_1e(t)]\chi(t),\\ \dot{V}(t) &\le \sum_{i=1}^{\mathcal{Q}}\tilde{\mathscr{X}}_i(\varrho(t))\sum_{j=1}^{\mathcal{Q}}\tilde{\mathscr{X}}_i^1(\varrho(l_sd)\Big[\chi^{\mathrm{T}}(t)\Big[\psi\\ &\quad + \eta_2\mathbb{W}\mathbb{G}_3^{-1}\mathbb{W}^{\mathrm{T}}]\chi(t) - \int_{t-\eta_2}^{t}[\chi^{\mathrm{T}}(t)\mathbb{W}\\ &\quad + \dot{\varrho}^{\mathrm{T}}(s)\mathbb{G}_3]\mathbb{G}_3^{-1}[\chi^{\mathrm{T}}(t)\mathbb{W} + \dot{\varrho}^{\mathrm{T}}(s)\mathbb{G}_3]^{\mathrm{T}}\mathrm{d}s\Big].\end{aligned}$$

Applying Schur complement $\Psi + \eta_2\mathbb{W}\mathbb{G}_3^{-1}\mathbb{W}^{\mathrm{T}} < 0$, is equivalent to

$$\Phi_1 = \begin{bmatrix} \Psi & \bar{\mathbb{W}} & \eta_1\mathbb{G}_1\hat{\Gamma}_1^{\mathrm{T}} & \eta_{12}\mathbb{G}_2\hat{\Gamma}_1^{\mathrm{T}} & \mathbb{S}_1\hat{\Gamma}_1^{\mathrm{T}} & \varpi_{16} \\ * & -\frac{1}{\eta_2}\mathbb{G}_3 & 0 & 0 & 0 & 0 \\ * & * & -\eta_1\mathbb{G}_1 & 0 & 0 & 0 \\ * & * & * & -\eta_{12}\mathbb{G}_2 & 0 & 0 \\ * & * & * & * & -\mathbb{S}_1 & 0 \\ * & * & * & * & * & \varpi_{66} \end{bmatrix}, \tag{27}$$

where
$\varpi_{16} = [\eth_1\ \eth_2\ \eth_3]$, $\varpi_{66} = \mathrm{diag}\{-\eta_2\mathbb{G}_3\ -\mathbb{G}_2\ -3\mathbb{G}_2\}$.
Moreover, the uncertain part is given as follows:

$$\Phi_1 + \overbrace{\begin{bmatrix} \mathbb{P}^T\mathbb{E}_i^T \\ \left.\begin{matrix}0\\0\\0\end{matrix}\right\}\text{14 times} \end{bmatrix}}^{\Gamma_d} \mathbb{F}(t) \overbrace{[\mathbb{V}_{1i} \underbrace{0\ 0\ 0}_{14\ times}]}^{\Gamma_e} + (*) + \overbrace{\begin{bmatrix} \left.\begin{matrix}0\\0\\0\end{matrix}\right\}\text{11 times} \\ \mathbb{G}_1^T\mathbb{E}_i^T \\ \mathbb{G}_2^T\mathbb{E}_i^T \\ \mathbb{S}_1^T\mathbb{E}_i^T \\ \mathbb{G}_3^T\mathbb{E}_i^T \end{bmatrix}}^{V_d}$$

$$\overbrace{\mathbb{F}(t)[0\ 0\ \mathbb{V}_{2i}\ \underbrace{0\ 0\ 0}_{4\ times}\ \mathbb{V}_{2i}\ \underbrace{0\ 0\ 0}_{7\ times}]}^{V_e} + (*)$$
$$\leq \Phi_1 + \lambda_1^{-1}\Gamma_d\Gamma_d^T + \lambda_1\Gamma_e^T\Gamma_e + \lambda_2^{-1}V_dV_d^T + \lambda_2V_e^TV_e.$$

By using Lemma 2.4 and Schur complement, we obtain LMIs (22a) and (22b). Therefore, we conclude that the system (18) is robust and asymptotically stable. This completes the proof. □

Remark 3.2 This criterion ensures robust asymptotic stabilization for an IT2 fuzzy system with time-varying delays ETC. In most of the literature, the authors have examined the $\mathscr{PV}$ system with simple stabilization conditions for fuzzy approaches without time-varying delays in [14, 34–36]. However, in real-life applications, there is always uncertainty about parameters and time-varying delays [27, 28]. Therefore, we take this fact into account.

3.1 Event-Triggered Stabilization Criteria

Theorem 3.3 *For given positive scalars $\eta_1, \eta_2, \lambda_1, \lambda_2$, and κ_1, the described $\mathscr{PV}$ system (18) is robust asymptotically stable, if there exist common matrices $\hat{\mathbb{P}} \in \mathbb{R}^{4n\times4n} > 0$, $\hat{\mathbb{Q}}_1 > 0$, $\hat{\mathbb{Q}}_2 > 0$, $\hat{\mathbb{G}}_1 > 0$, $\hat{\mathbb{G}}_2 > 0$, $\hat{\mathbb{S}}_1 > 0$, $\hat{\mathbb{G}}_3 > 0$, $\hat{\mathscr{S}} \in \mathbb{R}^{3n\times3n}$, $\hat{\mathscr{X}} \in \mathbb{R}^{3n\times n}$, $\hat{\mathscr{Y}} \in \mathbb{R}^{2n\times n}$, $\hat{\mathscr{W}} \in \mathbb{R}^{2n\times2n}$, $\hat{\mathbb{Y}}$, $\mathbb{T}$, and any matrix $\hat{\mathbb{N}}_l \in \mathbb{R}^{5n\times n}$, $\hat{\mathbb{M}}_l \in \mathbb{R}^{5n\times n}$, $\hat{\tilde{\Theta}}_1$, $\hat{\tilde{\Theta}}_2$, $L_j, l = 1, 2$, and $\eta(t) \in \{\eta_1, \eta_2\}$ satisfying the following LMIs*:

$$\begin{bmatrix} \Psi_{11} & \bar{\mathbb{W}} & \eta_1\tilde{\Gamma}_1^{\mathrm{T}} & \eta_{12}\tilde{\Gamma}_1^{\mathrm{T}} & \tilde{\Gamma}_1^{\mathrm{T}} & \tilde{\Lambda}_{11} \\ * & -\frac{1}{\eta_2}\hat{\mathbb{G}}_3 & 0 & 0 & 0 & 0 \\ * & * & -\eta_1\varpi & 0 & 0 & 0 \\ * & * & * & -\eta_{12}\varpi_1 & 0 & 0 \\ * & * & * & * & \hat{\mathbb{S}}_1 - 2\bar{P} & 0 \\ * & * & * & * & * & \tilde{\Lambda}_{22} \end{bmatrix} < 0, \tag{28a}$$

$$\begin{bmatrix} \Psi_{11} & \bar{\mathbb{W}} & \eta_1\tilde{\Gamma}_1^{\mathrm{T}} & \eta_{12}\tilde{\Gamma}_1^{\mathrm{T}} & \tilde{\Gamma}_1^{\mathrm{T}} & \tilde{\Lambda}_{11} \\ * & -\frac{1}{\eta_2}\hat{\mathbb{G}}_3 & 0 & 0 & 0 & 0 \\ * & * & -\eta_1\varpi & 0 & 0 & 0 \\ * & * & * & -\eta_{12}\varpi_1 & 0 & 0 \\ * & * & * & * & \hat{\mathbb{S}}_1 - 2\bar{P} & 0 \\ * & * & * & * & * & \tilde{\Lambda}_{22} \end{bmatrix} < 0, \tag{28b}$$

where

$$\begin{aligned}
\varsigma_s &= \mathscr{A}_i\bar{P}\varsigma_1 + \mathscr{B}_iL_j\varsigma_3 - \mathscr{B}_iL_j\varsigma_4, \quad \varpi = (\hat{\mathbb{G}}_1 - 2\bar{P}), \\
\hat{\Gamma}_1^{\mathrm{T}} &= [\bar{P}^{\mathrm{T}}\mathscr{A}_i\ 0\ \mathscr{B}_iL_j\underbrace{0\ 0\ 0}_{4\ \text{times}}\ -\mathscr{B}_iL_j]^{\mathrm{T}}, \quad \varpi_1 = (\hat{\mathbb{G}}_2 - 2\bar{P}), \\
\Psi_{11} &= \Big[\mathrm{Sym}(\varphi_1^{\mathrm{T}}\mathbb{P}\varphi_2) + \varsigma_1^{\mathrm{T}}\hat{\mathbb{Q}}_1\varsigma_1 - \varsigma_2^{\mathrm{T}}\hat{\mathbb{Q}}_1\varsigma_2 + \varsigma_2^{\mathrm{T}}\hat{\mathbb{Q}}_2\varsigma_2 \\
&\quad - \varsigma_4^{\mathrm{T}}\hat{\mathbb{Q}}_2\varsigma_4 - \eta_{12}\Big(\mathrm{Sym}(\hat{\mathbb{N}}_1\mathbb{E}_1 + \hat{\mathbb{N}}_2\mathbb{E}_2) + \mathrm{Sym}(\hat{\mathbb{M}}_1\mathbb{E}_3 \\
&\quad + \hat{\mathbb{M}}_2\mathbb{E}_4)\Big) + \Upsilon_{1,1}^{\mathrm{T}}\bigtriangledown_1\Upsilon_{1,1} - \frac{\pi^2}{4}[(\varsigma_1 - \varsigma_2)^{\mathrm{T}}\hat{\mathbb{S}}_1(\varsigma_1 - \varsigma_2) \\
&\quad + 2[\varsigma_1^{\mathrm{T}}\hat{\mathbb{Y}} + \varsigma_4^{\mathrm{T}}\hat{\mathbb{T}}][\varsigma_1 - \varsigma_4] + \kappa_1[\varsigma_3 - \varsigma_1]^{\mathrm{T}}\hat{\tilde{\Theta}}_2 \\
&\quad \times [\varsigma_3 - \varsigma_1] - \varsigma_1^{\mathrm{T}}\hat{\tilde{\Theta}}_1\varsigma_1, \eth_1 = [\eta_2\hat{\Gamma}_1^{\mathrm{T}}\ \underbrace{0\ 0\ 0}_{7\ \text{times}}], \\
\tilde{\Lambda}_{22} &= \mathrm{diag}\{-\eta_2(\hat{\mathbb{G}}_3 - 2\bar{P})\ -\hat{\mathbb{G}}_2 - 3\hat{\mathbb{G}}_2\ -\lambda_1I\ -\lambda_1I \\
&\quad -\lambda_2I\ -\lambda_2I\}
\end{aligned}$$

and the other elements are defined in Theorem 3.1. The control gain matrices are calculated by $\mathbb{K}_j = L_jP_1^{-1}$.

Proof From Theorem 3.1, we know that if (22a) and (22b) hold, the closed-loop system (18) is robust asymptotically stable. Then, before and after multiplying to (22a) and (22b) by $\mathrm{diag}\{\underbrace{P_1^{-1}\ P_1^{-1}\ P_1^{-1}}_{9\ \text{times}}\ \mathbb{G}_1^{-1}\ \mathbb{G}_2^{-1}\ \mathbb{S}_1^{-1}\ \mathbb{G}_3^{-1}P_1^{-1}\ P_1^{-1}\ \underbrace{I\ I\ I}_{4\ \text{times}}\}$, and letting

$$\begin{aligned}
&\bar{P} = P_1^{-1}, \quad L_j = \mathbb{K}_jP_1, \quad \hat{\mathbb{Q}}_1 = \bar{P}\mathbb{Q}_1\bar{P}, \quad \hat{\mathbb{Q}}_2 = \bar{P}\mathbb{Q}_2\bar{P}, \\
&\hat{\mathbb{G}}_1 = \bar{P}\mathbb{G}_1\bar{P}, \quad \hat{\mathbb{G}}_2 = \bar{P}\mathbb{G}_2\bar{P}, \quad \hat{\mathbb{G}}_3 = \bar{P}\mathbb{G}_3\bar{P}, \quad \hat{\mathbb{S}}_1 = \bar{P}\mathbb{S}_1\bar{P}, \\
&\hat{\mathbb{S}}_2 = \bar{P}\mathbb{S}_2\bar{P}, \quad \hat{\mathbb{N}}_{1n} = \bar{P}\mathscr{N}_{1n}\bar{P}, \quad \hat{\mathbb{M}}_{1n} = \bar{P}\mathscr{M}_{1n}\bar{P}, \\
&\hat{\mathbb{N}}_{2n} = \bar{P}\mathscr{N}_{2n}\bar{P}, \quad \hat{\mathbb{M}}_{2n} = \bar{P}\mathscr{M}_{2n}\bar{P}, \quad \hat{\mathscr{S}}_l = \bar{P}\mathscr{S}_l\bar{P}, \quad \hat{\mathscr{X}}_s = \bar{P}\mathscr{X}_s\bar{P}, \\
&\hat{\mathscr{Y}}_q = \bar{P}\mathscr{Y}_q\bar{P}, \quad \hat{\mathscr{W}}_r = \bar{P}\mathscr{W}_r\bar{P}, \quad \hat{\mathbb{Y}} = \bar{P}\hat{\mathbb{Y}}\bar{P}, \quad \hat{\mathbb{T}} = \bar{P}\hat{\mathbb{T}}\bar{P}, \\
&\hat{P}_s = \bar{P}P_s\bar{P}, \quad \hat{\tilde{\Theta}}_q = \bar{P}\tilde{\Theta}_q\bar{P}, \quad q = 1, 2, l = 1, 2, \ldots, 6, \\
&s, r = 1, 2, 3, \quad n = 1, 2, \ldots, 5, \quad s = 2, 3, 4, \ldots, 10.
\end{aligned}$$

Because the term $\mathbb{G}_1^{-1}$, $\mathbb{G}_2^{-1}$, $\mathbb{G}_3^{-1}$, $\mathbb{S}_1^{-1}$, $\hat{\mathbb{G}}_1 = \bar{P}\mathbb{G}_1\bar{P}$, $\hat{\mathbb{G}}_2 = \bar{P}\mathbb{G}_2\bar{P}$, $\hat{\mathbb{S}}_1 = \bar{P}\mathbb{S}_1\bar{P}$, $\hat{\mathbb{G}}_3 = \bar{P}\mathbb{G}_3\bar{P}$ are both in the

same LMIs, which is hard to solve, for this purpose to facilitate the design of ETC, we convert $\mathbb{G}_1^{-1}$, $\mathbb{G}_2^{-1}$, $\mathbb{S}_1^{-1}$ into the subsequent inequality with $\hat{\mathbb{G}}_1$, $\hat{\mathbb{G}}_2$, $\hat{\mathbb{S}}_1$ according to Lemma 2.5:

$$-\mathbb{G}_l^{-1} \le \hat{\mathbb{G}}_l - 2\bar{P}, \quad -\mathbb{S}_1^{-1} \le \hat{\mathbb{S}}_1 - 2\bar{P}, \quad l = 1, 2, 3.$$

That is if (28a) and (28b) holds, the closed-loop system (18) is robust and asymptotically stable with an ETC. This completes the proof. □

Remark 3.4 Notice that Theorem 3.2 gives an adequate condition to coplan the event-triggered controller (15) and the event-triggered scheme in the communication (13). If the LMIs (28a) and (28b) is feasible, the gain matrices $\mathbb{K}_j$ and the triggered matrices $\tilde{\Theta}_1, \tilde{\Theta}_2$ can be obtained.

Remark 3.5 Compared with the existing literature works [14, 34–36], we initially propose the IT2 fuzzy ETC scheme for the $\mathscr{PV}$ system. In addition, the IT2 fuzzy ETC method can save the limited network bandwidth and speed up information transmission. To improve the stability and stabilization condition of the $\mathscr{PV}$ system, by choosing the suitable T–S fuzzy rules with the information of η_1 and η_2 and can be represented in the following numerical example section.

4 Simulation Results

To confirm the applicability and performance of the suggested $\mathscr{PV}$ system-based ETC scheme and simulations are presented in this section. The block diagram of the proposed $\mathscr{PV}$ ETC scheme is shown in Fig. 2. We use the MATLAB toolbox to carry out the behavior of the $\mathscr{PV}$ system. In the evaluations of the previous section, the state equation of the $\mathscr{PV}$ system can be modeled by the following IT2 T–S fuzzy system.

$$\begin{aligned}\dot{\varrho}(t) = \sum_{i=1}^{4} \tilde{\mathscr{X}}_i(\varrho(t)) \sum_{j=1}^{4} \tilde{\mathscr{X}}_i^1(\varrho(l_s d)(\hat{\mathscr{A}}_i \varrho(t) \\ + \hat{\mathscr{B}}_i \mathbb{K}_j(\varrho(t-\eta(t)) - e(t))),\end{aligned} \tag{29}$$

where

$$\mathscr{A}_1 = \begin{bmatrix} -\frac{M}{\mathscr{L}} & \frac{1}{\mathscr{L}} & -\frac{\alpha + v_d - M_a\gamma}{\mathscr{L}} \\ -\frac{1}{\hat{C}_1} & 0 & 0 \\ 0 & 0 & 0 \end{bmatrix}, \quad \mathscr{A}_2 = \begin{bmatrix} -\frac{M}{\mathscr{L}} & \frac{1}{\mathscr{L}} & -\frac{\beta + v_d - M_a\gamma}{\mathscr{L}} \\ -\frac{1}{\hat{C}_1} & 0 & 0 \\ 0 & 0 & 0 \end{bmatrix},$$

$$\mathscr{A}_3 = \begin{bmatrix} -\frac{M}{\mathscr{L}} & \frac{1}{\mathscr{L}} & -\frac{\alpha + v_d - M_a\delta}{\mathscr{L}} \\ -\frac{1}{\hat{C}_1} & 0 & 0 \\ 0 & 0 & 0 \end{bmatrix}, \quad \mathscr{A}_4 = \begin{bmatrix} -\frac{M}{\mathscr{L}} & \frac{1}{\mathscr{L}} & -\frac{\beta + v_d - M_a\delta}{\mathscr{L}} \\ -\frac{1}{\hat{C}_1} & 0 & 0 \\ 0 & 0 & 0 \end{bmatrix},$$

$$\mathscr{B}_1 = \mathscr{B}_2 = \mathscr{B}_3 = \mathscr{B}_4 = \begin{bmatrix} 0 \\ \frac{1}{\hat{C}_1} \\ 0 \end{bmatrix}.$$

The membership functions are as follows.

$$\underline{\lambda}_1^1(\varrho_1(t)) = 1 - e^{\frac{-\varrho_1^2(t)}{1.2}}, \quad \underline{\lambda}_1^2(\varrho_1(t)) = 1 - e^{\frac{-\varrho_1^2(t)}{1.2}},$$
$$\underline{\lambda}_1^3(\varrho_1(t)) = 0.23e^{\frac{-\varrho_1^2(t)}{0.25}}, \quad \underline{\lambda}_1^4(\varrho_1(t)) = 0.23e^{\frac{-\varrho_1^2(t)}{0.25}},$$
$$\underline{\lambda}_2^1(\varrho_1(t)) = 0.5e^{\frac{-\varrho_1^2(t)}{0.25}}, \quad \underline{\lambda}_2^2(\varrho_1(t)) = 1 - e^{\frac{-\varrho_1^2(t)}{1.5}},$$
$$\underline{\lambda}_2^3(\varrho_1(t)) = 0.5e^{\frac{-\varrho_1^2(t)}{0.25}}, \quad \underline{\lambda}_2^4(\varrho_1(t)) = 1 - e^{\frac{-\varrho_1^2(t)}{1.5}},$$
$$\overline{\lambda}_1^1(\varrho_1(t)) = 1 - 0.23e^{\frac{-\varrho_1^2(t)}{0.25}}, \quad \overline{\lambda}_1^2(\varrho_1(t)) = 1 - 0.23e^{\frac{-\varrho_1^2(t)}{0.25}},$$
$$\overline{\lambda}_1^3(\varrho_1(t)) = e^{\frac{-\varrho_1^2(t)}{1.2}}, \quad \overline{\lambda}_1^4(\varrho_1(t)) = e^{\frac{-\varrho_1^2(t)}{1.2}},$$
$$\overline{\lambda}_2^1(\varrho_1(t)) = e^{\frac{-\varrho_1^2(t)}{1.2}}, \quad \overline{\lambda}_2^2(\varrho_1(t)) = 1 - 0.5e^{\frac{-\varrho_1^2(t)}{0.25}},$$
$$\overline{\lambda}_2^3(\varrho_1(t)) = e^{\frac{-\varrho_1^2(t)}{1.2}}, \quad \overline{\lambda}_2^4(\varrho_1(t)) = 1 - 0.5e^{\frac{-\varrho_1^2(t)}{0.25}},$$

and $\underline{\mathscr{X}}_i(t) = \overline{\mathscr{X}}_i(t) = 0.5$. The system parameters are taken as $0.5 \le \iota_{\mathscr{L}} \le 0.3, 0.4 \le \mathscr{V}_0 \le 0.2,\ 0.8 \le \eta(t) \le 0.5$ and the other parameters are represented in Table 1. For this case, our point is to illustrate that system (18) is robust and asymptotically stable with respect to parametric uncertainties $\mathbb{V}_{1i}$, $\mathbb{V}_{2i} = \text{diag}\{0.2, 0.2, 0.2\}$ and $\mathbb{E}_i = \text{diag}\{0.4, 0.4, 0.4\}$. Then solving the LMIs in Theorem 3.3 via MATLAB LMI toolbox, a typical calculation is addressed as follows:

Algorithm 1: Algorithm to solve the problem $\mathcal{PV}$

Step 1: Set the $\mathcal{PV}$ system model parameters $\mathcal{A}_i, \mathcal{B}_j$ and uncertain parameters $\mathbb{V}_{1i}, \mathbb{V}_{2i}, \mathbb{E}_i$.
Step 2: Use the triggered conditions and novel LKF techniques to construct the LMIs in Theorem 3.3
Step 3: Set the initial conditions η_1, η_2 and the constrained condition $\eta(t)$.
Step 4: Adjust the value of η_1 and η_2 to calculate whether the solution of LMI exists.
Step 5: If the feasible solution exists, stop the calculation and obtain the maximum value of η_2, the controller gains $\mathbb{K}_j$ and the event triggered parameters, else go to step 4 and increase or decrease the value of η_1 and η_2.
Step 6: Stop.

Using the above typical calculation, another arrangement of feasible solutions is obtained. In view of the feasible solutions, the equivalent event-triggered parameters, and gain matrices are calculated as follows can be estimated by

Table 1 Parameters of the $\mathscr{PV}$ system

Symbol	M	$\mathscr{L}$	$\hat{C}_1$	v_d	M_a
Value	35 (Ω)	40 mH	1 mF	1.9 V	0.05 (Ω)

$$\mathbb{K}_1 = [2.7823 \quad -5.8233 \; 6.0062],$$
$$\mathbb{K}_2 = [4.5841 \quad -3.5344 \; 5.2114],$$
$$\mathbb{K}_3 = [5.9119 \quad -2.3354 \; 10.7851],$$
$$\mathbb{K}_4 = [8.8245 \quad -6.1471 \; 12.5487],$$
$$\tilde{\Theta}_1 = \begin{bmatrix} 318.1440 & 4.7138 & -2.8686 \\ 4.7138 & 594.9665 & -0.1215 \\ -2.8686 & -0.1215 & 275.8819 \end{bmatrix},$$
$$\tilde{\Theta}_2 = \begin{bmatrix} 0.5328 & -0.1662 & -0.0238 \\ -0.1662 & 38.2215 & 0.0127 \\ -0.0238 & 0.0127 & 0.1582 \end{bmatrix}.$$

5 Simulation Results and Discussion

The proposed system's simulation results with a DC-to-DC boost converter are presented in this section. The DC/DC boost converter and the proposed controller are modeled using MATLAB/Simulink software. The proposed system with the boost converter is subject to both line and load variations and the corresponding results are presented. Line variations may occur due to the change in the environmental condition of the solar panel. The level of the irradiance falling on a solar panel and the operating temperature have a significant impact on the output of the solar panel, as shown in Fig. 3. Solar $\mathscr{PV}$ panels are rated based on standard test conditions with an irradiance of 1000 W/m^2 and a temperature of 25 °C. The DC-to-DC boost converter is expected to provide a constant output voltage to the load. As line and load conditions vary, the output voltage might also change accordingly. The reference DC voltage is compared with the actual output capacitor voltage, which is connected across the load, and the corresponding error signal is captured for analysis purposes. The load variations might happen due to sudden changes in the load's operating conditions or due to the increase in load demand. To capture the effectiveness of the proposed system during load variations, step variation in load is introduced, and the corresponding results are presented in Fig. 4.

5.1 Effect of Load Variations

A step variation in the load condition is introduced at 0.05 s, and the corresponding variations in state variables and controller input and output are also presented. The measured output load voltage is compared with the reference output voltage, and the error signal is shown in Fig. 4a. Measured state variables are referred to as a proposed control system, and the output of the fuzzy logic event-triggered controller (ETC) is shown in Fig. 4b. The fuzzy logic ETC output is utilized to generate the control signal, and the form of the duty cycle to the switching device S1 on the variations in the duty cycle is presented in Fig. 4c.

The control input to the DC-to-DC converter modifies the duty cycle of the switching device S1, which is translated to the corresponding changes in the state variable of the DC-to-DC boost converter. As presented in the previous sections, there are two state variables: the inductor current and the capacitor voltage. The continuous switching of the semiconductor switching device S1 introduces slight variations over the steady-state value of the state variable, which can be observed from the corresponding waveforms. The current waveform of the inductor is shown in Fig. 4d. Once the variation of the load step is revoked, the current drawn by the load changes must be supplied by the additional current drawn from the source. Since the additional current has to go through the inductor to reach the load, changes are observed in the inductor current. The

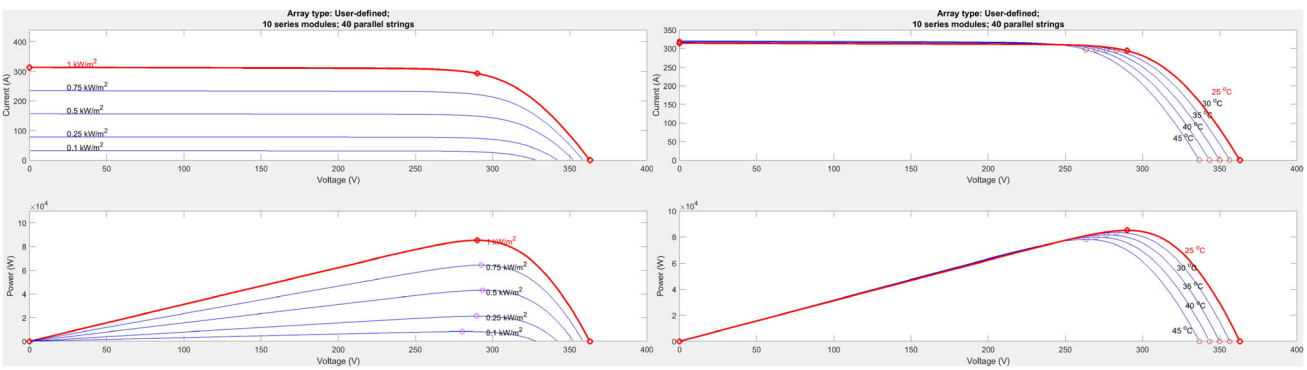

(a) Solar $\mathscr{PV}$ graphs with different irradiance

(b) Solar $\mathscr{PV}$ graphs with different temperatures

Fig. 3 Simulation results for P–V characteristic of the $\mathscr{PV}$ system

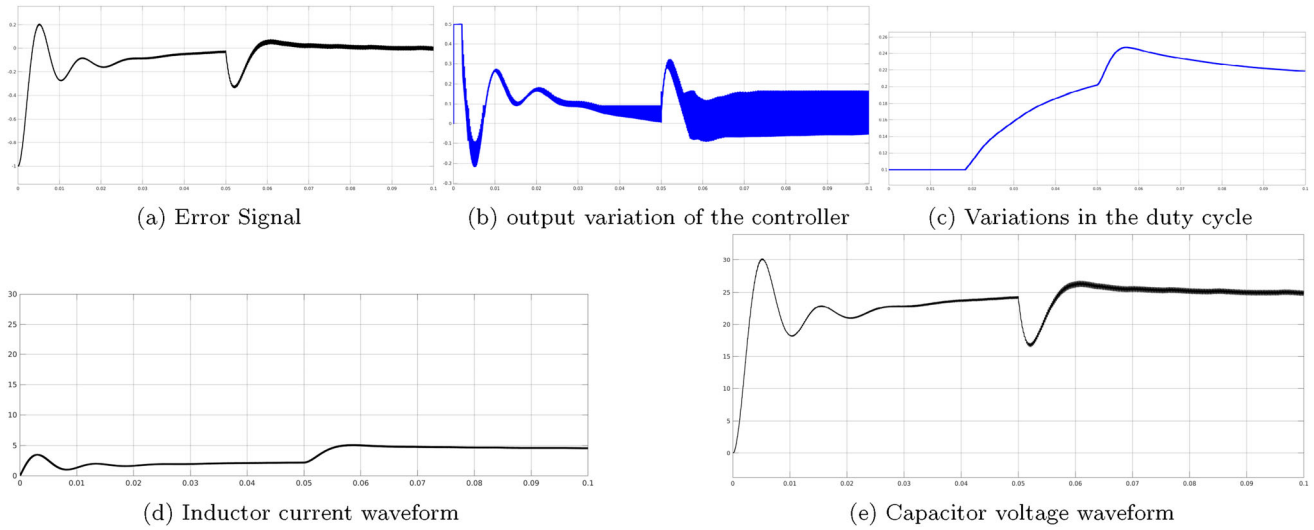

Fig. 4 Simulation results for the dynamic load test with a step variation in load

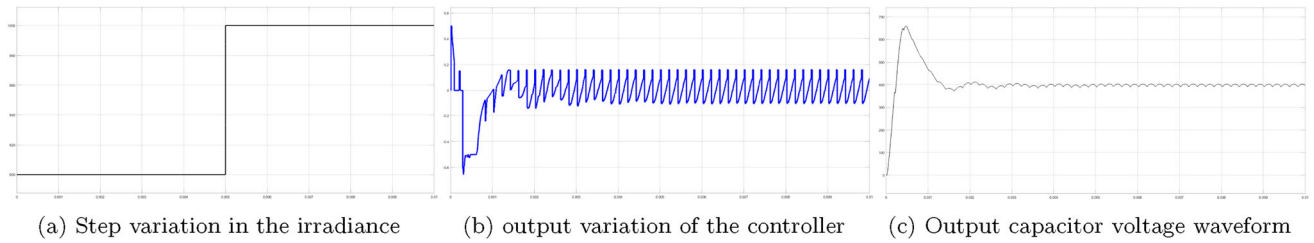

Fig. 5 Simulation results for the step variation in irradiance

inductor current once gets settled after the steady-state operation is perturbed why the load variation and reaches a new steady-state value after a time of 0.05 s.

The variations in the output voltage and response to a load-step variation are shown in Fig. 4d. Even though the capacitor is a state variable, it is directly connected across the DC load, and hence any modification in the load conditions causes an appropriate modification in the capacitor voltage as well. One can notice that the sudden variation load step causes a drop in the output voltage, and the voltage quickly rebounds to a steady-state value, which is testimony to the effectiveness of the proposed controller.

5.2 Effect of Line Variations

5.2.1 Variation in the Solar Irradiance Conditions

This section presents the results related to the line variations. The system considered in this work utilizes a solar $\mathscr{PV}$ panel as an input to the DC-to-DC boost converter. The solar $\mathscr{PV}$ panel converts the light energy to electricity, and hence any variations in the environmental conditions, including solar irradiance and temperature, shall have a definite impact on the regular operation of the DC to DC boost converter. In this context, the proposed system, along with the DC to DC boost converter, is subjected to two variations in the input conditions, such as solar irradiance and temperature, and the corresponding results are presented in Fig. 5. The intermittent nature of the environmental conditions under which a solar $\mathscr{PV}$ panel operates directly impacts the electrical output of the solar $\mathscr{PV}$ panel. The DC to DC boost converter's usage ensures constant DC voltage supply to the load under intermittent operating conditions. Out of the different environmental factors, solar irradiance falling On the panel and the solar panel's operating temperature are the major factors that influence the electrical output of a solar $\mathscr{PV}$ panel. The irradiance change is affected by the step variation, which is shown in Fig. 5a. The change in irradiation can be due to a passing cloud, deposition of dust particles on top of the Solar $\mathscr{PV}$ panel, partial shading of the Solar $\mathscr{PV}$ panel, or a specific change in the climatic condition. In any of the cases listed above, the worst change that could happen is a step variation used to study the proposed controller's performance. The response to the change in irradiation is in the form of a change in the duty cycle affected by the fuzzy

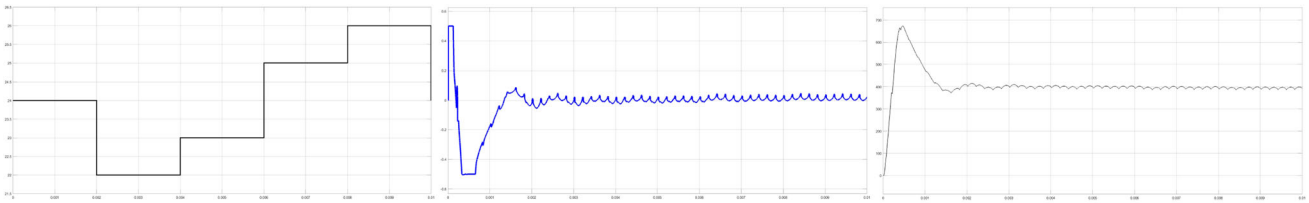

(a) Change in the input temperature profile (b) output variation of the controller (c) Output capacitor voltage waveform

Fig. 6 Simulation results for the dynamic temperature modifications

logic ETC output, which is shown in Fig. 5b. The corresponding output voltage for the step variation in the solar irradiance is shown in Fig. 5c. It can be observed from the waveforms that at time 0.05 s, solar irradiance is varied from 900 to 1000 W/m^2, and the output voltage stays relatively constant even during the varying input conditions.

5.2.2 *Effect of Partial Shading*

The solar PV panels' rated capacity depends on the standard testing conditions. If the standard irradiance value deviates from 1000 W/m^2, it might be due to two possible reasons. First, the panel could be experiencing partial shading, due to which some of the modules in the panel might not be producing output. Secondly, the irradiance falling on the panel could be changed due to the change in the environmental conditions [37]. In either case, the change in the voltage/current from the panel changes, thus modifying the internal impedance of the panel. The nominal operating point of the solar PV panel is the coinciding point of the load line on the P–V characteristics. If the solar PV panel is driving a constant load, the change in the panel's internal impedance must be matched with the constant load. A DC/DC converter is used to interface the solar PV panel and the load. By changing the duty cycle of the DC/DC converter, the effective impedance seen by the solar PV panel can be modified. Hence an interface DC/DC converter is used to match the solar PV panel impedance with the load impedance, thereby extracting maximum power from the solar PV panel. The DC/DC converter is also responsible for regulating the output voltage arising due to the line and load variations. In the case of partial shading, the irradiance falling on the panel changes, and hence the solar PV panel's internal impedance is modified. The controller response shall be in the form of a change in the duty cycle for impedance matching. For the change in the irradiance, the response in the duty cycle is observed in Fig. 5b. For any given panel with multiple modules, there is a critical point [38] beyond which a change in the partial shading shall not have a definitive impact on panel performance. The critical point is given by,

$$\text{Critical Point} \leq -1000 \times \frac{\text{Number of shaded modules}}{\text{Number of total modules}} + 900. \tag{30}$$

The solar PV panel considered in this work consists of 10 series modules and 40 parallel strings. If 5% of the modules are shaded, the critical point can be calculated as 850 W/m^2. Hence an irradiance value above the critical point is considered, and the step variation of irradiance from 900 to 1000 W/m^2 is introduced in the simulation model, as shown in Fig. 5a. For this change in irradiance, the controller is capable of maintaining a regulated output voltage by appropriately modifying the duty cycle, as shown in Fig. 5b. The output voltage is maintained constant irrespective of the change in the irradiance, as shown in Fig. 5c. Thus, the partial shading is treated as a line variation, and the DC/DC converter with the proposed controller can handle line variations due to partial shading.

5.2.3 *Variation in the Solar Panel Temperature Conditions*

The next variation that is considered in the input is the temperature change. The environment with temperature has a finite impact on the electrical output of a solar $\mathscr{PV}$ system to maintain the temperature within the safe operating region, several solutions like forced cooling, water spraying, and erection of solar $\mathscr{PV}$ system on top of water bodies are also considered in the real-world applications. For testing purposes and instead of a step variation in temperature, a temperature profile is considered as shown in Fig. 6a, and the response of the proposed system with temperature profile is presented. The proposed control system works to ensure constant output voltage for the DC load, and the corresponding control action is shown in Fig. 6b. The control action is translated to the duty cycle and is fed to the switching device S1. As the change in duty cycle directly impacts the state variables, the controller thrives on maintaining a constant voltage across the DC load, and the corresponding waveform is shown in Fig. 6c. The proposed controller portrays good performance with both line and load variations, which are observed from the results presented in this section.

Table 2 Comparison of the proposed controller based on different performance metrics

Control Algorithm	PV array dependency	Analog/ Digital	Convergence speed	Algorithm complexity	Parameters measured	Network delay considered	Utilization of communication resources
Perturb and Observe method [42]	No	Both	Vary	Low	Panel voltage and current	No	High
Incremental conductance method [43]	No	Digital	Vary	Medium	Voltage and current	No	High
Array reconfiguration [44]	Yes	Digital	Slow	High	Panel voltage and current	No	High
Type 2 FLC [45]	Yes	Digital	Vary	High	Panel voltage and current	No	High
Adaptive radial movement optimization [46]	Yes	Digital	Vary	High	Panel voltage and current	No	High
Particle Swarm Optimization algorithm [47]	Yes	Digital	Slow	Medium	Panel voltage and current	No	High
Ten check algorithm [48]	No	Digital	Slow	Medium		No	High
Proposed system	Yes	Digital	Fast	High	Panel voltage and current	Yes	Low

5.2.4 Hardware Implementation Issues

This section presents the hardware implementation issues of the proposed controller for the DC/DC Boost converter. For the selection of passive components, a 200 W power rating is considered. The inductor value is selected based on the equation derived from the volt-second balance technique [39] applied for the inductor.

$$\Delta \imath_{\mathscr{L}} = \mathscr{V}_{\mathscr{P}\mathscr{V}} \frac{D}{\mathscr{L} f_{\mathrm{sw}}}. \tag{31}$$

Similarly, the charge-second technique is applied to the output capacitor to find the value of the capacitor, which is given by,

$$\Delta \mathscr{V}_0 = \mathscr{V}_{\mathscr{P}\mathscr{V}} \frac{D}{R \times \hat{C}_2 \times f_{\mathrm{sw}}(1-u)}. \tag{32}$$

Using the above two equations, the inductor and capacitor values are found to be $\mathscr{L} = 40\,\mu\mathrm{H}$ and $\hat{C}_2 = 1000\,\mu\mathrm{H}$, respectively. The switching devices' voltage and current ratings are selected based on the switch positioning analysis, which is used to identify the blocking voltage and the conduction current for each switch. The operation quadrants of the switching device are determined based on voltage and current values, and the switching device is selected. The controlled switch (S_1) is a MOSFET, and the uncontrolled switch is a diode. The implementation of the proposed control algorithm requires a digital microcontroller system. For the purpose of rapid prototyping, the simulation model developed in MATLAB can be used. The OPAL-RT platform allows the rapid prototyping of digital control algorithm models developed using custom-made blocks available in the MATLAB toolbox. The proposed closed-loop control system requires the boost converter to measure state variables' values. Precisely the inductor current and the output voltage have to be measured. The measured signal should be properly filtered and scaled for the usage of the proposed controller. With appropriate sensors for measuring the state variables, the proposed controller can be implemented on the OPAL-RT platform with the real hardware running with the sensors feeding the measured values of state variables to the processor-in-the-loop and get the controller-determined duty cycle and, in turn, the PWM pulses to the proposed converter. The Embedded Coder toolbox can also be used to automatically generate the 'C' language code for the proposed controller, which can be used for implementation on a microcontroller platform.

5.2.5 Algorithm Performance Metrics

This section compares different metrics of the proposed control algorithm with well-established techniques available in the literature.

First, the convergence speed of a control algorithm denotes the amount of time required to reach the MPP. Besides the algorithm performance, the delay induced by the network or the algorithm affects the efficient tracking of the MPP. The controller will miss the intermittent irradiance level change if the delay introduced by the network is more than the time taken for the irradiance change. Since the proposed control

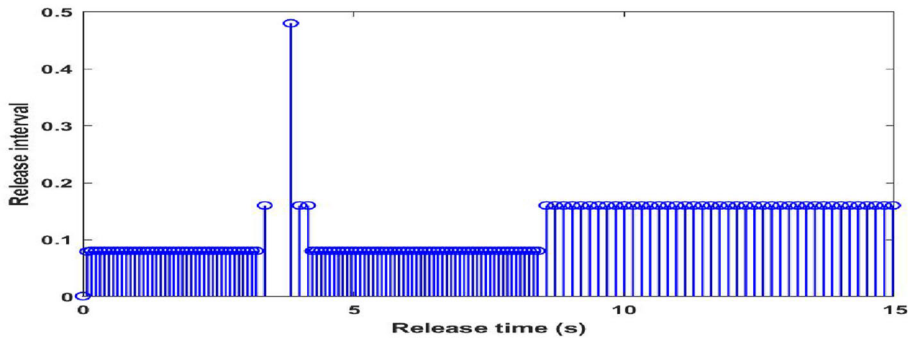

Fig. 7 Release intervals

algorithm considers network delay, it ensures asymptotic stabilization with ETC. The inbuilt command available in MATLAB named 'tic-toc' captures the convergence time of different control algorithms [40]. The convergence speed obtained for the proposed control algorithm is 1.1 ms. The convergence speed is quick for the proposed controller when compared to its counterpart. The comparison of the convergence time of the proposed controller with other conventional algorithms is presented in Table 2.

The proposed control algorithm is complex and requires a complex digital controller for implementation. The computational effort required to obtain the MPP is the major factor affecting the algorithm complexity. The proposed control algorithm includes the method to reduce the impact of communication delay in conjunction with MPP tracking. As a result of this, there will be an increase in the algorithm complexity. However, the event-triggered mechanism reduces the number of data transmissions in the channel while ensuring asymptotic stability. As a result of this, the computational effort increase introduced by the algorithm shall be compensated by the reduction of data transmission, thus saving the computational resources, as shown in Fig. 7. A comparison of the algorithm complexity of the proposed system, along with other conventional algorithms, is presented in Table 2.

The proposed system exhibits array dependency like the traditional FLC controller [40]. The exact data related to the panel configuration are required for the optimal operation of the proposed converter. These data are used in the controller development of the proposed system. PV array dependency of the FLC cannot be eliminated unless a numerical technique is considered [41].

In order to show better convergence for the MPP of the solar $\mathscr{PV}$ characteristics are utilizing the comparison with temperature and irradiance. The simulations effects have been pictured in Fig. 6. With the analysis of $\mathscr{PV}$ characteristics in Fig. 3, one can be seen that the effectiveness of the developed controller shows good dynamic response and superior performance. Furthermore, the release instants and release intervals are depicted in Fig. 7 with $t \in (0, 30]$. It can be seen that the event-triggered mechanism is used to reduce the number of data transmissions in the channel based on ensuring the stability analysis of the $\mathscr{PV}$ system. This helps to conserve network resources. In conclusion, the simulation research demonstrates that the controller based on the event-triggered mechanism created in this paper can not only stabilize the considered system but also minimize the communication network. The event-triggered mechanism and controller developed are validated.

6 Conclusion

In this article, an event-triggered approach has been proposed to stabilize the $\mathscr{PV}$ system with communication delay under the IT2 fuzzy model and uncertain parameters. The simulation results show a perfect accomplishment of the working point to the MPP activity with a satisfactory constant voltage activity. It can be concluded that the fuzzy ETC IT2 designed for the $\mathscr{PV}$ power framework improves the productivity of the extracted power. Based on the LMI approach with novel integral inequalities, the LMI-based sufficient conditions for the uncertain T–S fuzzy model with a prescribed performance are established. The main results prove that the proposed methodology guarantees asymptotic stability. Then, the desired controller gains and triggered parameters have been derived, which are expressed in terms of LMIs. Finally, simulation examples are given to verify the performance of the designed ETC IT2 fuzzy approach. Furthermore, the stabilization of nonlinear $\mathscr{PV}$ systems with Markovian switching parameters and disturbances is also the direction of our future work.

Acknowledgements The authors express their gratitude to the referees for their useful and constructive comments.

Author Contributions All authors contributed equally and significantly to writing this article and typed, read, and approved the final manuscript.

Funding This work was jointly supported by the National Natural Science Foundation of China (62173139) and the Science and Technology Innovation Program of Hunan Province (2021RC4030).

Data Availability Data sharing is not applicable to this article, as no data sets were generated or analyzed during the current study.

Declarations

Conflict of interest The authors declare that they have no conflict of interest concerning the publication of this manuscript.

References

1. Ueda, Y., Kurokawa, K., Tanabe, T., Kitamura, K., Sugihara, H.: Analysis results of output power loss due to the grid voltage rise in grid-connected photovoltaic power generation systems. IEEE Trans. Ind. Electron. **55**(7), 2744–2751 (2008)
2. Liserre, M., Sauter, T., Hung, J.Y.: Future energy systems: integrating renewable energy sources into the smart power grid through industrial electronics. IEEE Ind. Electron. Mag. **4**(1), 18–37 (2010)
3. Shafiullah, G.M., Oo, A.M.T., Jarvis, D., Ali, A.B.M.S., Wolfs, P.: Potential challenges: integrating renewable energy with the smart grid. In: 2010 20th Australasian Universities Power Engineering Conference, pp. 1–6. IEEE (2010)
4. Franco, I.B., Power, C., Whereat, J.: SDG 7 affordable and clean energy. In: Actioning the Global Goals for Local Impact, pp. 105–116. Springer, Singapore (2020)
5. Li, J., Chen, S., Wu, Y., Wang, Q., Liu, X., Qi, L., Lu, X., Gao, L.: How to make better use of intermittent and variable energy? A review of wind and photovoltaic power consumption in China. Renew. Sustain. Energy Rev. **137**, 110626 (2021)
6. Zainuri, M.A.A.M., Radzi, M.A.M., Soh, A.C., Abd Rahim, N.: Development of adaptive perturb and observe-fuzzy control maximum power point tracking for photovoltaic boost DC–DC converter. IET Renew. Power Gener. **8**(2), 183–194 (2013)
7. Sourov, M.R., Ahmed, U.T., Rabbani, M.G.: A high performance maximum power point tracker for photovoltaic power system using DC–DC boost converter. IOSR J. Eng. **2**(12), 12–20 (2012)
8. Salah, C.B., Ouali, M.: Comparison of fuzzy logic and neural network in maximum power point tracker for PV systems. Electr. Power Syst. Res. **81**(1), 43–50 (2011)
9. Liu, Y.-H., Liu, C.-L., Huang, J.-W., Chen, J.-H.: Neural-network-based maximum power point tracking methods for photovoltaic systems operating under fast changing environments. Sol. Energy **89**, 42–53 (2013)
10. Esram, T., Chapman, P.L.: Comparison of photovoltaic array maximum power point tracking techniques. IEEE Trans. Energy Convers. **222**(2), 439–449 (2007)
11. Femia, N., Petrone, G., Spagnuolo, G., Vitelli, M.: Optimization of perturb and observe maximum power point tracking method. IEEE Trans. Power Electron. **20**(4), 963–973 (2005)
12. Wang, T., Zhang, X., Li, Y.: Type-2 fuzzy adaptive event-triggered saturation control for photovoltaic grid-connected power systems. Int. J. Fuzzy Syst. **23**(4), 1150–1162 (2021)
13. Hiyama, T., Kouzuma, S., Imakubo, T.: Identification of optimal operating point of PV modules using neural network for real time maximum power tracking control. IEEE Trans. Energy Convers. **10**(2), 360–367 (1995)
14. Siraj Khan, M.M., Arifin, M., Haque, A., Al-Masood, N.: Stability analysis of power system with the penetration of photovoltaic based generation. Int. J. Energy Power Eng. **2**(2), 84–89 (2013)
15. Takagi, T., Sugeno, M.: Fuzzy identification of systems and its applications to modeling and control. IEEE Trans. Syst. Man Cybern. **1**, 116–132 (1985)
16. Assawinchaichote, W., Nguang, S.K., Shi, P.: Fuzzy Control and Filter Design for Uncertain Fuzzy Systems, vol. 347. Springer, Berlin (2007)
17. Sakthivel, N., Suruthi Sri, C.A., Zhai, G.: Finite-time extended dissipativity control for interval type-2 fuzzy systems with resilient memory sampled-data controller. J. Frankl. Inst. **359**(2), 1320–1346 (2022)
18. Parameswari, M., Nancy, P., Sathya Priya, J.: An energy-efficient routing framework using fuzzy type 2 hybrid Archimedes in wireless sensor network. Int. J. Fuzzy Syst. (2022). https://doi.org/10.1007/s40815-022-01397-7
19. Li, H., Tie, M., Wang, Y.: Event-triggered sliding mode control using the interval type-2 fuzzy logic for steer-by-wire systems with actuator fault. Int. J. Fuzzy Syst. **24**(7), 3104–3117 (2022)
20. Gao, Y., Li, H., Wu, L., Karimi, H.R., Lam, H.-K.: Optimal control of discrete-time interval type-2 fuzzy-model-based systems with D-stability constraint and control saturation. Signal Process. **120**, 409–421 (2016)
21. Wu, H., Mendel, J.M.: Uncertainty bounds and their use in the design of interval type-2 fuzzy logic systems. IEEE Trans. Fuzzy Syst. **10**(5), 622–639 (2002)
22. Li, X., Ye, D.: Memory-based dynamic event-triggered control for networked interval type-2 fuzzy systems subject to DoS attacks. Int. J. Adapt. Control Signal Process. **36**(1), 104–121 (2022)
23. Song, W., Tong, S.: Observer-based fuzzy event-triggered control for interval type-2 fuzzy systems. Int. J. Fuzzy Syst. **24**(1), 1–11 (2022)
24. Shanmugam, L., Joo, Y.H.: Design of interval type-2 fuzzy-based sampled-data controller for nonlinear systems using novel fuzzy Lyapunov functional and its application to PMSM. IEEE Trans. Syst. Man Cybern. Syst. **51**, 542–551 (2018)
25. Xie, L.: Output feedback H_∞ control of systems with parameter uncertainty. Int. J. Control **63**(4), 741–750 (1996)
26. Kwon, W., Koo, B., Lee, S.-M.: Novel Lyapunov–Krasovskii functional with delay-dependent matrix for stability of time-varying delay systems. Appl. Math. Comput. **320**, 149–157 (2018)
27. Sun, L., Tang, Y., Wang, W., Shen, S.: Stability analysis of time-varying delay neural networks based on new integral inequalities. J. Frankl. Inst. **357**(15), 10828–10843 (2020)
28. Vadivel, R., Joo, Y.H.: Robust event-triggered T–S fuzzy system with successive time-delay signals and its application. IET Control Theory Appl. **14**(20), 3697–3712 (2020)
29. Zhang, W., Wang, T., Tong, S.: Event-triggered control for networked switched fuzzy time-delay systems with saturated inputs. Int. J. Fuzzy Syst. **21**(5), 1455–1466 (2019)
30. Zhang, W., Wang, T., Tong, S.: Event-triggered control for networked switched fuzzy time-delay systems with saturated inputs. Int. J. Fuzzy Syst. **21**(5), 1455–1466 (2019)
31. Song, W., Tong, S.: Observer-based fuzzy event-triggered control for interval type-2 fuzzy systems. Int. J. Fuzzy Syst. **24**(1), 1–11 (2022)
32. Li, M., Zhao, J., Xia, J., Zhuang, G., Zhang, W.: Extended dissipative analysis and synthesis for network control systems with an event-triggered scheme. Neurocomputing **312**, 34–40 (2018)
33. Kaewpraek, N., Assawinchaichote, W.: H_∞ fuzzy state-feedback control plus state-derivative-feedback control synthesis for photovoltaic systems. Asian J. Control **18**(4), 1441–1452 (2016)
34. Ounnas, D., Ramdani, M., Chenikher, S., Bouktir, T.: An efficient maximum power point tracking controller for photovoltaic systems using Takagi–Sugeno fuzzy models. Arab. J. Sci. Eng. **42**(12), 4971–4982 (2017)

35. Youssef, F.B., Sbita, L.: Sliding mode control strategy for grid connected PV system. In: 2017 International Conference on Green Energy Conversion Systems (GECS), pp. 1–7. IEEE (2017)
36. Veerachary, M., Senjyu, T., Uezato, K.: Neural-network-based maximum-power-point tracking of coupled-inductor interleaved-boost-converter-supplied PV system using fuzzy controller. IEEE Trans. Ind. Electron. **50**(4), 749–758 (2003)
37. Patel, H., Agarwal, V.: Maximum power point tracking scheme for PV systems operating under partially shaded conditions. IEEE Trans. Ind. Electron. **55**(4), 1689–1698 (2008)
38. Teo, J.C., Tan, R.H.G., Mok, V.H., Ramachandaramurthy, V., Tan, C.K.: Impact of partial shading on the P–V characteristics and the maximum power of a photovoltaic string. Energies **11**(7), 1860 (2018)
39. Erickson, R.W., Maksimović, D.: Fundamentals of Power Electronics, 2nd edn. Springer, New York (2001)
40. Walker, S.S.W., Sooriyaarachchi, N.K., Liyanage, N.D.B., Abeynayake, P.A.G.S., Abeyratne, S.G.: Comparative analysis of speed of convergence of MPPT techniques. In: 2011 6th International Conference on Industrial and Information Systems, ICIIS 2011—Conference Proceedings, 2011, pp. 522–526 (2011)
41. Tofoli, F.L., De Castro Pereira, D., De Paula, W.J.: Comparative study of maximum power point tracking techniques for photovoltaic systems. Int. J. Photoenergy **2015**, 812582 (2015)
42. Podder, A.K., Roy, N.K., Pota, H.R.: MPPT methods for solar PV systems: a critical review based on tracking nature. IET Renew. Power Gener. **13**, 1615–1632 (2019)
43. Nadeem, A., Hussain, A.: A comprehensive review of global maximum power point tracking algorithms for photovoltaic systems. Energy Syst. (2021). https://doi.org/10.1007/s12667-021-00476-2
44. Ahmed, S., Mekhilef, S., Mubin, M.B., Tey, K.S.: Performances of the adaptive conventional maximum power point tracking algorithms for solar photovoltaic system. Sustain. Energy Technol. Assess. **53**, 102390 (2022)
45. Zhang, S., et al.: Maximum power point tracking control of solar power generation systems based on type-2 fuzzy logic. In: Proceedings of the World Congress on Intelligent Control and Automation (WCICA), September 2016, pp 770–774 (2016)
46. Seyedmahmoudian, M., Soon, T.K., Horan, B., Ghandhari, A., Mekhilef, S., Stojcevski, A.: New ARMO-based MPPT technique to minimize tracking time and fluctuation at output of PV systems under rapidly changing shading conditions. IEEE Trans. Ind. Inform. (2019). https://doi.org/10.1109/TII.2019.2895066
47. Kaced, K, Larbes, C, Ait-Chikh, SM, Bounabi, M, Dahmane, ZE: FPGA implementation of PSO based MPPT for PV systems under partial shading conditions. In: 2017 6th International Conference on Systems and Control (ICSC), 2017, pp. 150–155 (2017)
48. Awan, M.M.A., Javed, M.Y., Asghar, A.B., Ejsmont, K.: Performance optimization of a ten check MPPT algorithm for an off-grid solar photovoltaic system. Energies **15**, 2104 (2022)

R. Vadivel received the B.Sc., M.Sc., and M.Phil. Degrees in Mathematics from the Sri Ramakrishna Mission Vidyalaya College of Arts and Science affiliated to Bharathiar University, Coimbatore, India, in 2007, 2010, and 2012, respectively, and the PhD Degree from the Department of Mathematics, Thiruvalluvar University, Vellore, India, in 2018. He was a Postdoctoral Research Fellow with the Research Center for Wind Energy Systems, Kunsan National University, Gunsan, South Korea, from 2018 to 2019. He is currently working as a Lecturer with the Department of Mathematics, Faculty of Science and Technology, Phuket Rajabhat University, Phuket, Thailand.

T. K. Santhosh received the PhD Degree in Electrical Engineering from Anna University Chennai, in 2016, India. He was an Assistant Professor with the Knowledge Institute of Technology (KIOT), Salem, India. He is an Assistant Professor with the School of Electrical and Electronics Engineering, SASTRA Deemed University, Thanjavur, India. His research interest is the development of on-board power electronic converters and drive controllers for hybrid electric vehicle.

B. Unyong received the PhD Degree in Mathematics from Mahidol University, in 2004, Thailand. He was an Assistant Professor with the Department of Mathematics, Faculty of Science and Technology, Phuket Rajabhat University, Phuket, Thailand. He has experience and recipient funding from Thai Government. Currently he is working as an Associate Professor with the Department of Mathematics, School of Science, Walailak University, Thailand 80160. His research interests include mathematic model, epidemic diseases control model under the effect of climate change, oceanic model, atmospheric model, Lyapunov theory, and neural networks..

Quanxin Zhu received the M.S. Degree in Probability and Statistics from Hunan Normal University, Changsha, in 2002 and the PhD Degree in Probability and Statistics from Sun Yat-sen (Zhongshan) University, Guangzhou, China, in 2005. He is currently a Professor with Hunan Normal University, Distinguished Professor of Hunan Province and Leading Talent of Scientific and Technological Innovation in Hunan Province, Deputy Director of the Key Laboratory of Computing and Stochastic Mathematics of the Ministry of Education, and Director Control and Optimization of Complex Systems of Hunan Key Laboratory of Colleges and Universities. He won the Alexander von Humboldt Foundation of Germany and the Highly Cited Researcher Award by Clarivate Analytics in 2018–2021. He won First Prize of Hunan Natural Science Award and the list of Top 100000 Scientists in the world in 2020–2022. He is an Associate Editor of some international journals, the Lead Guest Editor of several journals, and a reviewer of more than 50 other journals. He is the author or the co-author of more than 300 journal articles. His research interests include stochastic control, stochastic systems, stochastic stability, stochastic delayed systems, Markovian jump systems, and stochastic complex networks.

Jinde Cao (Fellow, IEEE) received the B.S. Degree in Mathematics/Applied Mathematics from Anhui Normal University, Wuhu, China, in 1986, the M.S. Degree in Mathematics/Applied Mathematics from Yunnan University, Kunming, China, in 1989, and the PhD Degree in Mathematics/Applied Mathematics from Sichuan University, Chengdu, China, in 1998. He is currently an Endowed Chair Professor, the Dean of the School of Mathematics, the Director of the Jiangsu Provincial Key Laboratory of Networked Collective Intelligence of China and the Research Center for Complex Systems and Network Sciences, Southeast University, Nanjing, China. Professor Cao is elected as a Member of the Academy of Europe and the European Academy of Sciences and Arts, a Foreign Member of the Russian Academy of Natural Sciences and the Lithuanian Academy of Sciences, a Fellow of the Pakistan Academy of Sciences and the African Academy of Sciences, and an IASCYS Academician. He was a Recipient of the National Innovation Award of China, the Obada Prize, and the Highly Cited Researcher Award in Engineering, Computer Science, and Mathematics by Thomson Reuters/Clarivate Analytics.

Nallappan Gunasekaran received the PhD Degree in Mathematics/from Thiruvalluvar University, Vellore, India, in 2018. He was a Junior Research Fellow with the Department of Science and Technology-Science and Engineering Research Board (DST-SERB), Government of India, New Delhi, India. He was a Post-doctoral Research Fellow in the Research Center for Wind Energy Systems, Kunsan National University, Gunsan, South Korea, from 2017 to 2018. He was a Post-doctoral Research Fellow in Department of Mathematical Sciences, Shibaura Institute of Technology, Saitama, Japan, from 2018 to 2020. Currently, he is working as a Post-doctoral Research Fellow in Computational Intelligence Laboratory, Toyota Technological Institute, Japan. His research interests are deep learning, natural language processing, complex dynamical networks, and cryptography, etc. Dr. Gunasekaran serves as a Reviewer for various SCI journals. He has authored and co-authored of more than 70 research articles in various SCI journals.